GEÇİCİ KAPAK

Kapak tasarımı
devam ediyor.

BİDGE Yayınları

Advances ın Computatıonal Chemıstry and Molecular Structure Analysıs

Editör: ABDULLAH GÖKTAŞ

ISBN: -

1. Baskı
Sayfa Düzeni: Gözde YÜCEL
Yayınlama Tarihi: -
BİDGE Yayınları

Sertifika No: 71374
Yayın hakları © BİDGE Yayınları
www.bidgeyayinlari.com.tr - bidgeyayinlari@gmail.com
Krc Bilişim Ticaret ve Organizasyon Ltd. Şti.
Güzeltepe Mahallesi Abidin Daver Sokak Sefer Apartmanı No: 7/9 Çankaya / Ankara

İÇİNDEKİLER

BÖLÜM 0

DFT SİMÜLASYONLARINDA DEĞİŞ-TOKUŞ KORELASYON FONKSİYONELLERİNİN VE SÖZDE-POTANSİYELLERİN KARŞILAŞTIRMALI ANALİZİ

Eşe Akpınar[1]

Giriş

Yoğunluk fonksiyonel teorisi (Density Functional Theory, DFT), etkileşimli çok-elektron problemini elektron yoğunluğu $\rho(r)$ üzerinden yeniden formüle ederek, dış potansiyel $v(r)$ altındaki temel durum enerjisinin yoğunluk fonksiyoneli olarak minimize edilebileceğini gösteren çerçeveye dayanır (Hohenberg & Kohn, 1964). Hohenberg–Kohn teoremleri, $v(r)$'den bağımsız evrensel bir yoğunluk fonksiyoneli $F[n]$ bulunduğunu ve $E \equiv \int v(r)n(r)\,dr + F[n]$ ifadesinin doğru temel durum yoğunluğunda minimum verdiğini ispatlar (Hohenberg & Kohn, 1964; Kohn & Sham, 1965). Bu kavramsal temel, malzeme bilimi ve katıhal fiziğinde yaygın olarak kullanılan, periyodik sistemlerin temel durum özelliklerini hesaplamaya yönelik öz-tutarlı denklemlerin türetilmesine doğrudan zemin sağlar (Lejaeghere et al., 2016).

[1] Dr., Isparta Uygulamalı Bilimler Üniversitesi, İleri Teknolojiler Anabilim Dalı, Orcid: 0000-0003-0632-2150

DFT'nin pratik gücü, değiş-tokuş korelasyon (exchange-correlation, XC) enerjisinin uygun bir yaklaşımla modellenmesine bağlıdır; çünkü Kohn–Sham formülasyonu, etkileşimli sistemin karmaşıklığını XC katkısı üzerinden tek bir fonksiyonel terime yoğunlaştırır (Lejaeghere et al., 2016). Bu nedenle XC seçimi, özellikle bant aralığı gibi elektronik yapıya duyarlı büyüklüklerde belirleyici olabilir: saf (yarı-yerel) fonksiyonellerin bant aralıklarını sistematik olarak küçümsediği bilinmekte olup bu eksiklik, özellikle yarıiletken ve yalıtkan sistemlerde belirgin hale gelmektedir (Perdew & Schmidt, 2001). Buna karşılık taralı hibrit (screened hybrid) HSE yaklaşımının bu hatayı belirgin biçimde azalttığı ve saf fonksiyonellere kıyasla bant aralığı tahminlerinde önemli iyileşme sağladığı gösterilmiştir (Heyd et al., 2003).

Bu bölümün amacı, periyodik katıhal sistemlerinde DFT simülasyonlarının iki kritik bileşeni olan (i) XC fonksiyoneli ve (ii) sözde-potansiyel (pseudopotential, PP) yaklaşımını birlikte ele alarak, hangi hedef özellikler için hangi seçimlerin daha rasyonel olduğuna dair yorumlayıcı bir çerçeve sunmaktır (Lejaeghere et al., 2016). Önce Kohn–Sham DFT'nin temel denklemleri verilecek, ardından Jacob merdiveni (Jacob's ladder) sınıflaması üzerinden XC aileleri (LDA, GGA, meta-GGA, hibrit ve dispersiyon düzeltmeleri) fiziksel içgörü ve hesaplama maliyeti bağlamında karşılaştırılacaktır (Perdew & Schmidt, 2001; Sun et al., 2015). Sonrasında norm-koruyan (norm-conserving), ultrasoft ve PAW yaklaşımları tartışılarak PP seçiminde aktarılabilirlik ve sayısal yakınsama temaları öne çıkarılacaktır (Vanderbilt, 1990). Son bölümde ise literatürden seçili kıyaslamalar üzerinden 2B malzemeler ve oksitler bağlamında XC/PP seçimlerinin sonuçlara yansıması fiziksel olarak yorumlanacak; ardından pratik bir karar rehberi tablo halinde özetlenecektir (Rekik et al., 2024).

Teorik Çerçeve

Hohenberg–Kohn yaklaşımı, dış potansiyel v(r) altındaki etkileşimli elektron gazının temel durumunu ele alır ve yoğunluk üzerinden evrensel bir fonksiyonel bulunduğunu ortaya koyar (Hohenberg & Kohn, 1964). Bu yaklaşım, enerji minimizasyonu ilkesiyle birlikte DFT'nin varyasyonel temelini oluşturur (Hohenberg & Kohn, 1964; Kohn & Sham, 1965).

Kohn–Sham DFT

Kohn–Sham (KS) yaklaşımı, Hohenberg–Kohn teoremlerinden hareketle inhomojen etkileşimli elektron sistemi için öz-tutarlı denklemler geliştirir (Kohn & Sham, 1965). KS çerçevesinde toplam enerji fonksiyoneli tipik olarak aşağıdaki biçimde yazılır; burada T_s etkileşimsiz kinetik enerji, E_H Hartree elektrostatik enerjisi, E_{XC} ise değiş-tokuş ve korelasyon katkısını temsil eder (Kohn & Sham, 1965):

$$E_\rho \;=\; T_s[\rho] \;+\; E_H[\rho] \;+\; E_{XC}[\rho] \;+\; \int v_{ext}(r)\,\rho(r)\,dr$$

KS tek-elektron denklemleri, öz-tutarlı çözüm gerektiren bir özdeğer problemine indirgenir (Kohn & Sham, 1965):

$$\left(-\frac{1}{2}\nabla^2 \;+\; v_{eff}(r)\right)\psi_i(r) \;=\; \varepsilon_i\psi_i(r)$$

Bu formülasyonda efektif potansiyel aşağıdaki gibi tanımlanır; burada v_{XC} terimi, uniform elektron gazının değiş-tokuş ve korelasyon katkılarının efektif potansiyeller olarak sisteme dahil edildiği şekilde ortaya çıkar (Kohn & Sham, 1965):

$$v_{eff}(r) \;=\; v_{ext}(r) \;+\; v_H(r) \;+\; v_{XC}(r)$$

XC potansiyeli ise fonksiyonel türevle tanımlanır; bu nedenle pratik hesaplamalar için E_{XC}'ye ilişkin seçilen yaklaşık form, tüm KS çözümünü belirleyici hale getirir (Kohn & Sham, 1965):

$$v_{XC}(r) = \frac{\delta E_{XC}[\rho]}{\delta \rho(r)}$$

Öz-Tutarlı Alan Döngüsü

KS denklemleri öz-tutarlı alan (self-consistent field, SCF) döngüsüyle çözülür; başlangıç yoğunluğu $\rho(r)$ ile v_{eff} kurulur, özdeğer problemi çözülerek $\{\psi_i\}$ elde edilir ve yeni yoğunluk güncellenerek yakınsama sağlanana dek iterasyon sürdürülür (Kohn & Sham, 1965). Bu sürecin kararlılığı ve yakınsama davranışı, XC fonksiyonelinin sayısal özellikleri ve seçilen hesaplama parametreleriyle yakından ilişkilidir. Topluluk ölçekli kıyaslamalar, güncel kod ve sözde-potansiyellerin çoğu kez birbirleriyle çok iyi uyum gösterebildiğini, ancak eski yaklaşımların daha az kesin sonuçlar üretebildiğini belirtir (Lejaeghere et al., 2016).

XC Fonksiyonelleri

XC fonksiyonelleri, artan karmaşıklık ve (çoğu problem sınıfı için) artan doğruluk hedefiyle "Jacob merdiveni" metaforu altında sınıflandırılır (Perdew & Schmidt, 2001). Merdivenin alt basamakları daha yerel bilgiye dayanırken, üst basamaklar daha fazla yerel/yarı-yerel girdi veya açıkça orbital bağımlı terimler içerir; bu ilerleme, çoğu durumda hesaplama maliyetini de artırır (Perdew & Schmidt, 2001; Sun et al., 2015).

LDA

Yerel yoğunluk yaklaşımı (Local Density Approximation, LDA), XC enerjisini, her noktada homojen elektron gazı referansına dayalı yerel bir enerji yoğunluğu üzerinden yaklaşıklar (Kohn & Sham, 1965). Bu yaklaşımın fiziksel sezgisi, gerçek sistemin her uzay noktasında "yerel olarak homojen" kabul edilmesidir; dolayısıyla XC katkısı, o noktadaki yoğunlukla aynı yoğunluğa sahip uniform elektron gazının bilinen değiş-tokuş ve korelasyon enerjisiyle temsil edilir (Kohn & Sham, 1965). Katılarda gözlenen

sistematik eğilimler bağlamında, LDA'nın çoğu durumda kafes sabitlerini küçümseme (underestimate) eğilimi olduğu ve kohezyon enerjilerini fazla tahmin etme davranışı gösterdiği değerlendirilmiştir (Zhang et al., 2018). Bu eğilim, homojen elektron gazı referansının bağlanmayı "fazla güçlendiren" yönlü bir hata üretmesiyle tutarlı biçimde açıklanabilir (Zhang et al., 2018). Bununla birlikte LDA, basit metallerde ve yoğun iyonik katılarda elektron yoğunluğunun gerçekten yavaş değiştiği durumlarda makul sonuçlar üretebilmekte; düşük hesaplama maliyeti ve sayısal kararlılığı nedeniyle özellikle ön-hesaplama (ön hesaplama) ve kıyaslama amaçlı kullanımlarda referans başlangıç noktası olarak tercih edilmeye devam etmektedir (Lejaeghere et al., 2016).

GGA

Genelleştirilmiş gradyan yaklaşımı (Generalized Gradient Approximation, GGA), XC enerjisini yoğunluğa ek olarak yoğunluk gradyanına bağlı hale getirerek LDA'nın aşırı yerelliğini azaltmayı amaçlar (Perdew & Schmidt, 2001). PBE (Perdew–Burke–Ernzerhof) bu sınıfta en yaygın örneklerden biridir ve GGA'ların LDA'ya kıyasla atomlar, moleküller ve katılarda iyileştirme sunduğu vurgulanır (Perdew et al., 1996). Bununla birlikte, PBE'nin kafes sabitlerini fazla tahmin edip, bulk modülünü küçük tahmin etme eğilimi olduğu rapor edilmiştir (Zhang et al., 2018). Bu nedenle PBEsol gibi "katılar için PBE" varyantları, özellikle yavaş değişen yoğunluklar için kafes sabitleri ve yüzey enerjilerinde iyileşme hedefler (Perdew et al., 2008).

meta-GGA

meta-GGA sınıfı, GGA girdilerine ek olarak kinetik enerji yoğunluğu gibi ek yerel büyüklükleri dahil ederek farklı bağ türlerini ayırt etme kapasitesini artırmayı hedefler (Sun et al., 2015). SCAN (Strongly Constrained and Appropriately Normed) yaklaşımı, meta-GGA için bilinen 17 kesin kısıtı sağlama iddiasıyla tasarlanmış ve

özellikle kafes sabitleri ile zayıf etkileşimlerde dikkate değer doğruluk sağladığı bildirilmiştir (Sun et al., 2015). SCAN'ın, çoğu zaman hibrit fonksiyonellerle karşılaştırılabilir doğruluk sağlarken neredeyse GGA maliyetinde çalışabildiği de vurgulanır (Sun et al., 2016). Yüksek verimli (yüksek verimli) hesaplamalar açısından r²SCAN, SCAN'ın sayısal yakınsama sorunlarını azaltmak ve geniş veri setlerinde daha güvenilir yakınsama sunmak üzere tercih edilen bir varyant olarak değerlendirilmektedir (Kingsbury et al., 2022).

Hibrit Fonksiyoneller

Hibrit fonksiyoneller, değiş-tokuş enerjisinin belirli bir kısmını Hartree–Fock benzeri tam değiş-tokuş ile karıştırarak, özellikle bant aralığı gibi büyüklüklerde yarı-yerel yaklaşımların sistematik eksiklerini azaltmayı hedefler (Perdew & Schmidt, 2001). Ekranlanmış hibrit HSE yaklaşımı, Coulomb operatörünü kısa ve uzun menzilli bileşenlere ayırır ve yalnızca kısa menzilde HF değiş-tokuşunu dahil ederek metal ve dar bant aralıklı sistemlerde görülebilen fiziksel olmayan uzun menzilli etkileri azaltmayı amaçlar (Heyd et al., 2003). HSE'nin katılarda bant aralıkları için saf fonksiyonellere göre belirgin hata azalımı sağladığı ve hesaplama maliyetinin saf fonksiyonellere göre çoğu durumda yalnızca ~2–4 kat arttığı rapor edilmiştir (Heyd et al., 2003; Perdew et al., 1996).

Dispersiyon Düzeltmeleri

Semilokal KS-DFT'nin uzun menzilli korelasyon etkilerini, özellikle dispersiyon/van der Waals etkileşimlerini, çoğu fonksiyonelde yeterince tanımlayamadığı vurgulanır; bu eksikliği gidermek için D3 gibi eklemeli dispersiyon düzeltmeleri yaygın biçimde kullanılır (Grimme et al., 2010). DFT-D3 yaklaşımı, KS-DFT enerjisine bir dispersiyon terimi ekleyerek $E_{DFT-D3} = E_{KS-DFT} + E_{disp}$ şeklinde uygulanır ve dispersiyon enerjisinin iki-cisim ile üç-cisim katkılarından oluştuğu belirtilir (Grimme et al., 2010; Ehlert, 2024):

$$E_{\text{DFT-D3}} = E_{\text{KS-DFT}} + E_{disp}$$

Tkatchenko–Scheffler (TS) yaklaşımı ise dispersiyon parametrelerini yerel elektronik çevreye duyarlı biçimde yoğunluktan türetmeyi hedefleyen bir ölçekleme çerçevesi sunar (Tkatchenko & Scheffler, 2009). TS düzeltmelerinin bazı katılarda bağlanma enerjilerini deneysel değerlere kıyasla fazla tahmin edebildiği ve özellikle iyonik sistemlerde ek iyileştirme gerektirebileceği belirtilmiştir (Bučko et al., 2013).

Bu bölümde tartışılan XC ailelerinin özet bir karşılaştırması Tablo 3.1'de verilmiştir.

Tablo 3.1. Yaygın XC yaklaşımlarının özet özellikleri.

Basamak	**Örnek**	**Fiziksel İçerik**	**Tipik Artı-Eksi**	**Göreli Maliyet**
LDA	LDA	Homojen elektron gazı referansı	Kafes sabitini küçümseme, kohezyonu fazla tahmin etme (Zhang et al., 2018)	1×
GGA	PBE	ρ ve ∇ρ; LSD'ye göre iyileşme (Perdew et al., 1996)	Kafes sabitlerini fazla tahmin etme (Zhang et al., 2018)	~1×
GGA	PBEsol	Katılar için gradyan açılımını geri kazandırma (Perdew et al., 2008)	Kafes/yüzey iyileşmesi; atomizasyon enerjilerinde kötüleşme riski	~1×
meta-GGA	SCAN	17 kesin kısıt; yüksek doğruluk (Sun et al., 2015)	Hibrit doğruluğuna yakın performans, GGA maliyeti	~1–2×
meta-GGA	r²SCAN	Güvenilir yakınsama; yüksek verimli uygunluğu	SCAN'a yakın doğruluk, daha iyi sayısal stabilite	~1–2×

Basamak	Örnek	Fiziksel İçerik	Tipik Artı-Eksi	Göreli Maliyet
		(Kingsbury et al., 2022)		
Hibrit	HSE	Kısa menzilde HF değiş-tokuşu (Heyd et al., 2003)	Bant aralığı tahminlerinde belirgin iyileşme; maliyet 2–4×	2–4×
Dispersiyon	D3	Eklemeli dispersiyon: E_2 + E_3 (Grimme et al., 2010)	Uzun menzilli korelasyonun düşük maliyetle dahil edilmesi	Düşük ek

Kaynak: Yazarlar tarafından literatürden derlenerek hazırlanmıştır.

Sözde-Potansiyel Formalizmleri

Düzlem dalga tabanlı periyodik hesaplamalarda, çekirdek bölgesindeki hızlı salınımlı dalga fonksiyonlarını doğrudan temsil etmek büyük baz setleri gerektirebilir; sözde-potansiyel yaklaşımları bu yükü azaltmak için çekirdek elektronlarını etkin potansiyele gömer (Vanderbilt, 1990; Blöchl, 1994). Bu bölümde norm-koruyan, ultrasoft ve PAW formalizmleri aktarılabilirlik ve yakınsama perspektifiyle özetlenir (Vanderbilt, 1990).

Norm-Koruyan Yaklaşım

Norm-koruyan sözde-potansiyeller (Norm-Conserving Pseudopotentials, NCPP), bir kesme yarıçapı r_c dışında sözde ve tüm-elektron dalga fonksiyonlarının eşleşmesi koşuluyla üretilir (Hamann, 2013). Transferabilite açısından kritik olan norm-koruma koşulu aşağıdaki biçimde ifade edilir; burada $\varphi(r)$ tüm-elektron, $\varphi_{PS}(r)$ ise sözde dalga fonksiyonunu temsil eder (Hamann, 2013):

$$\int_0^{r_c} |\phi(r)|^2 \, r^2 \, dr = \int_0^{r_c} |\phi_{PS}(r)|^2 \, r^2 \, dr$$

Modern norm-koruyan tasarımlarda optimize norm-koruyan Vanderbilt (ONCV) yaklaşımı, daha düşük kesim enerjilerinde

yakınsayan ve çoğu durumda daha doğru NCPP'ler üretme avantajı sunabilir (Schlipf & Gygi, 2015). Büyük ölçekli test çerçeveleri olarak PseudoDojo, ONCVPSP yaklaşımıyla üretilmiş geniş bir sözde-potansiyel tablosunu sistematik test bataryalarıyla doğrulayıp üretim hesapları için kesim enerjisi önerileri sağlamak üzere tasarlanmıştır (van Setten et al., 2018).

Ultrasoft Yaklaşım

Vanderbilt'in ultrasoft (US) yaklaşımı, norm-koruma kısıtının uygulanmadığı ve genelleştirilmiş bir özdeğer probleminin ortaya çıktığı, düzlem dalga tabanlı katıhal hesaplamalarına uygun ayrılabilir bir sözde-potansiyel formalizmi sunar (Vanderbilt, 1990). Bu formalizmde aktarılabilirliğin kesme yarıçapı sabit tutulsa bile sistematik olarak geliştirilebilmesi hedeflenir (Vanderbilt, 1990). USPP'lerin yüksek verimli hesaplamalar açısından pratik değerine dair örnek olarak, bazı kütüphanelerin tek bir düşük düzlem dalga kesimiyle kafes sabitleri, bulk modülleri ve manyetik momentlerde iyi genel doğruluk verdiği ifade edilmiştir; bununla birlikte dağıtılan üretim girdilerinin kalite garantisi olmadığı gibi uyarılar da açıkça belirtilmektedir (Kresse & Joubert, 1999).

PAW

Projektör artırılmış dalga (Projector Augmented-Wave, PAW) yöntemi, sözde-potansiyel yaklaşımı ile LAPW yaklaşımını doğal biçimde genelleyen bir elektronik yapı hesaplama çerçevesi olarak tanımlanır (Blöchl, 1994). PAW'nin ana fikri, sözde dalga fonksiyonundan tüm-elektron dalga fonksiyonuna bir dönüşümle erişmektir; genişletmenin lokalize projektörlerle örtüşüm üzerinden tanımlandığı vurgulanır (Blöchl, 1994). PAW dönüşümü aşağıdaki biçimde özetlenebilir:

$$|\psi\rangle = |\psi_{PS}\rangle + \sum \left(|\varphi_i\rangle - |\varphi_i^{PS}\rangle\right)\langle p_i|\psi_{PS}\rangle$$

Bu ifade, sözde dalga fonksiyonuna çekirdek bölgesinde tüm-elektron düzeltme terimlerinin eklendiği fikrini taşır ve PAW'nin doğruluk–maliyet dengesini açıklamak için kullanışlıdır (Blöchl, 1994). PAW'nin, birçok malzemede yapısal özellikleri PAW, LAPW ve sözde-potansiyel formalizmlerinin benzer doğrulukta temsil edebildiği rapor edilmiştir (Holzwarth et al., 1997; Torrent et al., 2010).

Bu üç yaklaşımın pratik bir karşılaştırması Tablo 4.1'de özetlenmiştir.

Tablo 4.1. PP formalizmlerinin karşılaştırılması.

Yaklaşım	Temel Fikir	Güçlü Yön	Kritik Uyarı
NCPP	Süreklilik ve norm-koruma; saçılma özelliklerini yeniden üretme (Hamann, 2013)	Geniş kod uyumluluğu ve iyi tanımlı formalizm	Transferabilite enerji aralığına duyarlı; kesim gereksinimi artabilir (Schlipf & Gygi, 2015)
USPP	Norm-koruma yok; genelleştirilmiş özdeğer problemi; düzlem dalga için ayrılabilir form (Vanderbilt, 1990)	Daha düşük kesimle verimlilik; yüksek verimli için uygun kütüphaneler mevcut	PP üretim kalitesi garanti olmayabilir; kütüphane uyarılarını takip etmek gerekir (Kresse & Joubert, 1999)
PAW	PP ve LAPW'yi genelleyen genişletme yaklaşımı; projektörlerle tanımlı dönüşüm (Blöchl, 1994)	Çekirdek bölgesi duyarlı büyüklüklerde güçlü performans; çoğu malzemede AE'ye yakın doğruluk	Uygulama ayrıntıları (ör. XC katkılarında sayısal hassasiyet) sonuçları etkileyebilir (Torrent et al., 2010)

Kaynak: Yazarlar tarafından literatürden derlenerek hazırlanmıştır.

XC ve PP Seçim Kriterleri

XC ve PP seçimi, yalnızca tek tek "iyi" seçenekleri bilmekten çok, hedef özelliğe göre hata kaynaklarını yönetmek anlamına gelir (Perdew et al., 1996; Lejaeghere et al., 2016). Topluluk ölçekli

kıyaslamalar, modern kodlar ve sözde-potansiyeller arasında sonuçların genel olarak iyi uyum gösterebildiğini, ancak bu uyumun bir kıyaslama çerçevesi içinde belgelendirilmesinin önemli olduğunu ifade eder (Lejaeghere et al., 2016).

Hedefe Göre XC Seçimi

Yapısal özellikler, kafes sabiti, bulk modülü gibi, çoğu katı için PBE ve PBEsol gibi GGA aileleriyle makul bir doğruluk düzeyinde öngörülebilir (Zhang et al., 2018; Perdew et al., 2008). Daha yüksek doğruluk hedefleniyorsa SCAN gibi meta-GGA'ların, çok çeşitli bağ türlerinde geometri ve enerji doğruluğunu artırabildiği ve çoğu durumda hibrit fonksiyonellerle rekabet edebildiği rapor edilmiştir (Sun et al., 2016). Elektronik yapı özelinde, özellikle bant aralığı için yarı-yerel fonksiyonellerin belirgin eksik tahmin eğilimi birçok kaynakta vurgulanır (Perdew et al., 2017). Bu nedenle hibrit yaklaşımı, özellikle HSE, bant aralığı odaklı hesaplarda güçlü bir adaydır (Heyd et al., 2003). Zayıf etkileşimler için dispersiyon katkılarının kritik olabildiği ve D3 gibi düzeltmelerin etkin biçimde kullanıldığı vurgulanır (Grimme et al., 2010; Ehlert, 2024).

DFT+U Yaklaşımı

Geçiş metal oksitleri gibi güçlü korelasyonlu sistemlerde, standart yarı-yerel DFT yaklaşımlarının elektron öz-etkileşimi ve bant aralığı eksikliği nedeniyle zorlayıcı olduğu açıkça belirtilmiştir (Dudarev et al., 1998). Geçiş metal oksitlerinde LSDA'nın güçlü Coulomb itmesini yetersiz betimlemesi sonucu metalik temel durum öngörebildiği ve deneysel yalıtkan davranışı kaçırabildiği vurgulanır (Dudarev et al., 1998). Bu bağlamda LSDA+U/DFT+U yaklaşımının, örneğin NiO'da 3d kabuk korelasyonlarını daha iyi hesaba katarak hem elektron enerji kaybı spektrumları hem de yapısal kararlılık parametrelerinde iyileştirme sağlayabildiği gösterilmiştir (Dudarev et al., 1998).

PP Seçimi

PP seçiminde birinci kriter, seçilen PP setinin sistematik testlerden geçmiş olması ve üretim hesapları için pratik kesim enerjisi önerileri sunmasıdır; PseudoDojo çerçevesi bu amaçla, ONCVPSP ile üretilmiş geniş bir tabloyu çok sayıda test bataryasıyla değerlendirip kesim önerileri sağlamak üzere tasarlanmıştır (van Setten et al., 2018). Ek olarak, sözde-potansiyellerde "hayalet (ghost) durumlar" gibi sayısal/temsil kaynaklı sorunların, özellikle GW ve optik özellikler gibi uygulamalarda yanlış sonuçlara yol açabileceği belirtilmiştir (Schlipf & Gygi, 2015).

Tablo 5.1, kod türleri ile tipik XC–PP–dispersiyon kombinasyonlarına yönelik pratik bir özet sunmaktadır.

Tablo 5.1. *DFT kodları için pratik XC–PP seçim örnekleri.*

Kod Tipi	**Tipik Baz**	**PP Yaklaşımı**	**XC İçin Pratik Başlangıç**	**Not**
Düzlem dalga	Düzlem dalga	PAW/USPP/NCPP (Vanderbilt, 1990; Blöchl, 1994)	PBE/PBEsol; bant aralığı için HSE (Heyd et al., 2003)	Dispersiyon için D3 eklenebilir (Grimme et al., 2010)
Atomik orbital	Yerel orbital	(Koda bağlı) PP türevleri	PBE/SCAN; yüksek verimli için r²SCAN (Kingsbury et al., 2022)	Yakınsama kontrolleri kritik (Lejaeghere et al., 2016)

Kaynak: Yazarlar tarafından literatürden derlenerek hazırlanmıştır.

Literatürden Karşılaştırmalı Bulgular

Literatürdeki karşılaştırmalı çalışmalar, XC seçimlerinin yapısal ve elektronik özelliklerde sistematik eğilimler ürettiğini ve bu eğilimlerin çoğu zaman fiziksel olarak yorumlanabilir olduğunu ortaya koyar (Zhang et al., 2018). Bu bölümde odak, 2B malzemeler ve bir oksit örneği üzerinden, LDA/GGA/meta-GGA/hibrit

seçimlerinin neden farklı sonuçlar verdiğini yorumlamaktır (Rekik et al., 2024).

2B Malzemeler

2B sistemlerde, özellikle bant aralığı ve uyarılmış durum özellikleri, hesaplamanın sayısal ayrıntılarına karşı hassas olabilir. Örneğin monolayer MoS_2 üzerinde yapılan GW çalışmaları, kesilmiş Coulomb etkileşiminin interlayer screening etkisini önlemek için gerekli olduğunu; aksi halde G_0W_0 bant aralıklarının ortalama ~0.5 eV kadar düşük çıkabildiğini rapor etmiştir (Pisarra et al., 2021). Semilokal DFT'nin bant aralığı tahminindeki yetersizliği daha genel bir olgu olarak rapor edilir; DFT bant aralığı ile deneysel kuaziparçacık bant aralığının karıştırılmaması gerektiği hatırlatılır (Perdew et al., 2017). Spesifik bir örnek olarak, 1H-MoS_2 için HSE ile bant aralığının 2.35 eV bulunabildiği rapor edilmiştir (Rai et al., 2020).

Oksitler

Oksitler özelinde, standart yarı-yerel yaklaşımların bant aralığı eksik tahmini ve öz-etkileşim kaynaklı polaronik etkiler nedeniyle kusur hesaplarında özellikle zorlayıcı olabildiği açıkça belirtilmiştir (Kowalski et al., 2010). TiO_2 örneğinde, HSE06 ekranlanmış hibrit fonksiyonelinin hem temel durum özelliklerinde hem de kusur durumları için güçlü performans gösterebildiği rapor edilmiştir (Deskins et al., 2011). Bant aralığı açısından daha doğrudan bir örnek olarak, rutil TiO_2 için HSE06 ile 3.12 eV bant aralığı elde edildiği ve bu değerin deneysel ~3.05 eV ile iyi uyum gösterdiği rapor edilmiştir (Janotti et al., 2010).

Bu bölümdeki kıyaslamaların pratik özeti Tablo 6.1'de nitel ve nicel referanslarla derlenmiştir.

Tablo 6.1. Seçili sistemler üzerinden literatür bulgularının özeti.

Sistem	Yöntem	Bulguların Özeti
Monolayer MoS_2	HSE	Bant aralığı 2.35 eV olarak rapor edilmiştir (Rai et al., 2020).
Monolayer MoS_2	GGA/mBJ	Bazı yarı-yerel yaklaşımların düşük bant aralığı verdiği ifade edilmiştir (Rekik et al., 2024).
Monolayer MoS_2	G_0W_0 yakınsama	Truncated Coulomb kullanılmazsa bant aralığı ortalama ~0.5 eV düşük çıkabilir; 45×45 k-ızgarasıyla ~0.1 eV yakınsama hedeflenir (Pisarra et al., 2021).
Rutil TiO_2	HSE06	3.12 eV hesaplanan bant aralığı, deneysel ~3.05 eV ile uyumlu rapor edilmiştir (Janotti et al., 2010).
TiO_2 kusurları	HSE06	HSE06'nın TiO_2 modifikasyonlarında doğru gap ve kusur düzeyleri için güvenilirlik sağladığı belirtilmiştir (Deskins et al., 2011; Kowalski et al., 2010).

Kaynak: Yazar tarafından literatürden derlenerek hazırlanmıştır.

Sonuç

Bu bölümde DFT'nin yoğunluk temelli evrensel fonksiyonel fikrine dayandığı ve Kohn–Sham öz-tutarlı denklemlerinin değiş-tokuş ve korelasyon katkılarını efektif potansiyel üzerinden sisteme dahil ettiği gösterilmiştir (Hohenberg & Kohn, 1964; Kohn & Sham, 1965). XC fonksiyoneli seçiminde LDA ve PBE gibi yarı-yerel yaklaşımların yapısal özelliklerde makul sonuçlar verebilmesine rağmen bant aralığı gibi büyüklüklerde sistematik hatalar üretebildiği; HSE gibi ekranlanmış hibritlerin ise bant aralığı hatalarını belirgin biçimde azaltabildiği ve maliyeti çoğu durumda 2–4 kat düzeyinde tuttuğu tartışılmıştır (Heyd et al., 2003; Zhang et al., 2018). Dispersiyon etkileşimleri için D3 ve TS gibi düzeltmelerin, yarı-yerel KS-DFT'nin uzun menzilli korelasyon eksikliğini pratik maliyetle giderebildiği vurgulanmıştır (Grimme et al., 2010; Tkatchenko & Scheffler, 2009). PP tarafında ise NCPP/USPP/PAW yaklaşımlarının farklı doğruluk–maliyet dengeleri sunduğu; modern tabloların sistematik testler ve kesim

önerileriyle seçim sürecini daha güvenilir hale getirdiği gösterilmiştir (van Setten et al., 2018).

Sonuç ve Pratik Tavsiyeler

Pratikte, yapısal özellikler için PBE/PBEsol veya SCAN/r²SCAN gibi yarı-yerel yaklaşımlarla başlayıp, hedef büyüklüğe göre (özellikle bant aralığı için) HSE gibi hibritlere geçmek rasyonel bir stratejidir (Heyd et al., 2003; Perdew et al., 2008). 2B sistemlerde ve uyarılmış durum hesaplarında yakınsama ayrıntılarının sonuçları ~0.1–0.5 eV ölçeğinde etkileyebileceği unutulmamalıdır (Pisarra et al., 2021). Dispersiyonun önemli olduğu sistemlerde D3 gibi eklemeli düzeltmeler veya yoğunluk temelli vdW şemaları kullanılmalı; ancak bazı sınıflarda (özellikle iyonik sistemlerde) aşırı bağlanma gibi risklere karşı doğrulama yapılmalıdır (Bučko et al., 2013). Sözdepotansiyel seçimi, sistematik testlerden geçmiş kütüphanelerle yapılmalı ve hedef uygulama (GW/optik gibi boş uzay hassasiyeti) "hayalet durum" türü sorunlara karşı özellikle kontrol edilmelidir (Schlipf & Gygi, 2015; van Setten et al., 2018).

Bölüm boyunca tartışılan seçimlerin hızlı bir karar tablosu olarak özeti Tablo 7.1'de verilmiştir.

Tablo 7.1. *Hedef özelliğe göre pratik karar rehberi.*

Hedef Özellik	Önerilen XC	Önerilen PP	Kritik Uyarı
Kafes parametresi	PBEsol veya SCAN/r²SCAN (Perdew et al., 2008; Sun et al., 2015)	PAW veya testli NCPP tabloları (Blöchl, 1994; van Setten et al., 2018)	PBE'nin kafes sabitlerini büyük tahmin eğilimi olabilir (Zhang et al., 2018)
Bant aralığı	HSE (screened hybrid) (Heyd et al., 2003)	PAW/USPP (kod uyumuna göre) (Vanderbilt, 1990; Blöchl, 1994)	Saf DFT fonksiyoneller bant aralığını ciddi küçümseyebilir (Perdew et al., 2017)

Hedef Özellik	Önerilen XC	Önerilen PP	Kritik Uyarı
Adsorpsiyon enerjisi	PBE + D3 (veya benzeri dispersiyon düzeltmesi) (Grimme et al., 2010)	PAW/NCPP (Blöchl, 1994; Hamann, 2013)	Semilokal DFT dispersiyonu kaçırır; düzeltme şarttır (Grimme et al., 2010)
Manyetik sistemler	SCAN veya PBE (+U gerekebilir) (Sun et al., 2015; Dudarev et al., 1998)	PAW (çekirdek bölgesi duyarlılığı için) (Blöchl, 1994)	Geçiş metal oksitlerinde yarı-yerel yaklaşımlar metalik durum öngörebilir (Dudarev et al., 1998)
2B malzemeler	HSE veya uygun yarı-yerel + dikkatli yakınsama (Heyd et al., 2003; Pisarra et al., 2021)	Testli PP + yakınsama odaklı seçim (van Setten et al., 2018)	k-ızgarası ve truncated Coulomb seçimi kritik olabilir (Pisarra et al., 2021)
Yüksek verimli tarama	r²SCAN (numerik stabilite) (Kingsbury et al., 2022)	USPP/NCPP tablosu (kesim önerili) (van Setten et al., 2018; Kresse & Joubert, 1999)	PP kalitesi ve uyarılar takip edilmeli; yakınsama belgelensin (Lejaeghere et al., 2016)

Kaynak: Yazar tarafından literatürden derlenerek hazırlanmıştır.

Kaynakça

Blöchl, P. E. (1994). Projector augmented-wave method. Physical Review B, 50(24), 17953–17979. https://doi.org/10.1103/PhysRevB.50.17953

Bučko, T., Lebègue, S., Hafner, J., & Ángyán, J. G. (2013). Tkatchenko-Scheffler van der Waals correction method with and without self-consistent screening applied to solids. Physical Review B :Condensed Matter and Materials Physics, 87(6), 064110. https://doi.org/10.1103/PhysRevB.87.064110

Deskins, N. A., Rousseau, R., & Dupuis, M. (2011). Distribution of Ti^{3+} surface sites in reduced TiO_2. Journal of Physical Chemistry C, 115(15), 7562–7572. https://doi.org/10.1021/jp2001139

Dudarev, S. L., Botton, G. A., Savrasov, S. Y., Humphreys, C. J., & Sutton, A. P. (1998). Electron-energy-loss spectra and the structural stability of nickel oxide: An LSDA+U study. Physical Review B, 57(3), 1505–1509. https://doi.org/10.1103/PhysRevB.57.1505

Ehlert, S. (2024). Simple DFT-D3: Library first implementation of the D3 dispersion correction. Journal of Open Source Software, 9(103), 7169. https://doi.org/10.21105/joss.07169

Grimme, S., Antony, J., Ehrlich, S., & Krieg, H. (2010). A consistent and accurate ab initio parametrization of density functional dispersion correction (DFT-D) for the 94 elements H-Pu. Journal of Chemical Physics, 132(15), 154104. https://doi.org/10.1063/1.3382344

Hamann, D. R. (2013). Optimized norm-conserving Vanderbilt pseudopotentials. Physical Review B, 88(8), 085117. https://doi.org/10.1103/PhysRevB.88.085117

Heyd, J., Scuseria, G. E., & Ernzerhof, M. (2003). Hybrid functionals based on a screened Coulomb potential. Journal of Chemical Physics, 118(18), 8207–8215. https://doi.org/10.1063/1.1564060

Hohenberg, P., & Kohn, W. (1964). Inhomogeneous electron gas. Physical Review, 136(3B), B864–B871. https://doi.org/10.1103/PhysRev.136.B864

Holzwarth, N. A. W., Matthews, G. E., Dunning, R. B., Tackett, A. R., & Zeng, Y. (1997). Comparison of the projector augmented-wave, pseudopotential, and linearized augmented-plane-wave formalisms for density-functional calculations of solids. Physical Review B, 55(4), 2005. https://doi.org/10.1103/PhysRevB.55.2005

Janotti, A., Varley, J. B., Rinke, P., Umezawa, N., Kresse, G., & Van de Walle, C. G. (2010). Hybrid functional studies of the oxygen vacancy in TiO_2. Physical Review B Condensed Matter and Materials Physics, 81(8), 085212. https://doi.org/10.1103/PhysRevB.81.085212

Kingsbury, R., Gupta, A. S., Bartel, C. J., Munro, J. M., Dwaraknath, S., Horton, M., & Persson, K. A. (2022). Performance comparison of r²SCAN and SCAN metaGGA density functionals for solid materials via an automated, yüksek verimli computational workflow. Physical Review Materials, 6(1), 013801. https://doi.org/10.1103/PhysRevMaterials.6.013801

Kohn, W., & Sham, L. J. (1965). Self-consistent equations including exchange and correlation effects. Physical Review, 140(4A), A1133–A1138. https://doi.org/10.1103/PhysRev.140.A1133

Kowalski, P. M., Camellone, M. F., Nair, N. N., Meyer, B., & Marx, D. (2010). Charge localization dynamics induced by oxygen

vacancies on the TiO_2(110) surface. Physical Review Letters, 105(14), 146405. https://doi.org/10.1103/PhysRevLett.105.146405

Kresse, G., & Joubert, D. (1999). From ultrasoft pseudopotentials to the projector augmented-wave method. Physical Review B, 59(3), 1758–1775. https://doi.org/10.1103/PhysRevB.59.1758

Lejaeghere, K., Bihlmayer, G., Björkman, T., Blaha, P., Blügel, S., Blum, V., Caliste, D., Castelli, I. E., Clark, S. J., Dal Corso, A., de Gironcoli, S., Deutsch, T., Dewhurst, J. K., Di Marco, I., Draxl, C., Dułak, M., Eriksson, O., Flores-Livas, J. A., Garrity, K. F., … Cottenier, S. (2016). Reproducibility in density functional theory calculations of solids. Science, 351(6280), aad3000. https://doi.org/10.1126/science.aad3000

Perdew, J. P., Burke, K., & Ernzerhof, M. (1996). Generalized gradient approximation made simple. Physical Review Letters, 77(18), 3865–3868. https://doi.org/10.1103/PhysRevLett.77.3865

Perdew, J. P., Ruzsinszky, A., Csonka, G. I., Vydrov, O. A., Scuseria, G. E., Constantin, L. A., Zhou, X., & Burke, K. (2008). Restoring the density-gradient expansion for exchange in solids and surfaces. Physical Review Letters, 100(13), 136406. https://doi.org/10.1103/PhysRevLett.100.136406

Perdew, J. P., & Schmidt, K. (2001). Jacob's ladder of density functional approximations for the exchange-correlation energy. AIP Conference Proceedings, 577(1), 1–20. https://doi.org/10.1063/1.1390175

Perdew, J. P., Yang, W., Burke, K., Yang, Z., Gross, E. K. U., Scheffler, M., Scuseria, G. E., Henderson, T. M., Zhang, I.

Y., Ruzsinszky, A., Peng, H., Sun, J., Trushin, E., & Görling, A. (2017). Understanding band gaps of solids in generalized Kohn-Sham theory. Proceedings of the National Academy of Sciences, 114(11), 2801–2806. https://doi.org/10.1073/pnas.1621352114

Pisarra, M., Díaz, C., & Martín, F. (2021). Theoretical study of structural and electronic properties of 2H-phase transition metal dichalcogenides. Physical Review B, 103(19), 195416. https://doi.org/10.1103/PhysRevB.103.195416

Rai, D. P., Vu, T. V., Laref, A., Patra, P. K., & Shankar, A. (2020). Promising optoelectronic response of 2D monolayer MoS_2: A first principles study. Chemical Physics, 538, 110824. https://doi.org/10.1016/j.chemphys.2020.110824

Rekik, N., Falfoul, Y., Issaoui, N., Ghalla, H., Oujia, B., & Al-Dossary, O. M. (2024). Compilation and deciphering MoS_2's physical properties: Accurate benchmark DFT simulations and assessment of advanced quantum methods. Chemical Physics, 579, 112229. https://doi.org/10.1016/j.chemphys.2024.112229

Schlipf, M., & Gygi, F. (2015). Optimization algorithm for the generation of ONCV pseudopotentials. Computer Physics Communications, 196, 36–44. https://doi.org/10.1016/j.cpc.2015.05.011

Sun, J., Remsing, R. C., Zhang, Y., Sun, Z., Ruzsinszky, A., Peng, H., Yang, Z., Paul, A., Waghmare, U., Wu, X., Klein, M. L., & Perdew, J. P. (2016). Accurate first-principles structures and energies of diversely bonded systems from an efficient density functional. Nature Chemistry, 8(9), 831–836. https://doi.org/10.1038/nchem.2535

Sun, J., Ruzsinszky, A., & Perdew, J. P. (2015). Strongly constrained and appropriately normed semilocal density functional. Physical Review Letters, 115(3), 036402. https://doi.org/10.1103/PhysRevLett.115.036402

Tkatchenko, A., & Scheffler, M. (2009). Accurate molecular van der Waals interactions from ground-state electron density and free-atom reference data. Physical Review Letters, 102(7), 073005. https://doi.org/10.1103/PhysRevLett.102.073005

Torrent, M., Holzwarth, N. A. W., Jollet, F., Harris, D., Lepley, N., & Xu, X. (2010). Electronic structure packages: Two implementations of the projector augmented wave (PAW) formalism. Computer Physics Communications, 181(10), 1862–1867. https://doi.org/10.1016/j.cpc.2010.07.036

Vanderbilt, D. (1990). Soft self-consistent pseudopotentials in a generalized eigenvalue formalism. Physical Review B, 41(11), 7892–7895. https://doi.org/10.1103/PhysRevB.41.7892

van Setten, M. J., Giantomassi, M., Bousquet, E., Verstraete, M. J., Hamann, D. R., Gonze, X., & Rignanese, G.-M. (2018). The PseudoDojo: Training and grading a 85 element optimized norm-conserving pseudopotential table. Computer Physics Communications, 226, 39–54. https://doi.org/10.1016/j.cpc.2018.01.012

Zhang, G.-X., Reilly, A. M., Tkatchenko, A., & Scheffler, M. (2018). Performance of various density-functional approximations for cohesive properties of 64 bulk solids. New Journal of Physics, 20(6), 063020. https://doi.org/10.1088/1367-2630/aac7f0

BÖLÜM 0

METHODOLOGICAL APPROACH QUANTUM CHEMICAL CALCULATIONS AND HIRSHFELD SURFACE ANALYSIS OF 3-BENZYL-2*H*-CHROMEN-2-ONE

CEM CÜNEYT ERSANLI[1]

Introduction

The study of naturally existing substances as well as the functions of these substances within ecosystems is currently one of the focal areas of modern biotechnology research. The coumarin derivatives, which are strategically important among the secondary metabolites of terrestrial flora, have been receiving special attention not only due to their medicinal properties but also because of their ability to form complicated structures. In this regard, the compound 3-benzyl-2*H*-chromen-2-one obtained from the seeds of the plant *Clausena lansium*, which is extensively employed in Chinese traditional medicine, presents an excellent subject for quantum chemical calculations due to the benzyl substitution in its coumarin ring structure. As part of this investigation, the geometry

[1] Prof. Dr., Sinop University, Faculty of Arts and Science, Department of Physics, Sinop/Turkey, Orcid: 0000-0002-8113-5091, ccersanli@sinop.edu.tr, ccersanli@gmail.com

of the molecules was optimized to obtain the ground state geometry of the molecules; also, atomic charges were analyzed by the Mulliken and natural population analysis (NPA) methods. Specifically, the NPA treatment of intramolecular charge transfer is superior to the Mulliken approach in terms of basis set insensitivity. Moreover, HOMO (Highest Occupied Molecular Orbital) and LUMO (Lowest Unoccupied Molecular Orbital) energies, which are essential for determining global reactivity parameters like the chemical hardness and softness of the molecule, were analyzed, together with molecular electrostatic potential (MEP) profiles for identifying reactive sites. Intermolecular interaction analysis, especially hydrogen bonding and $\pi\cdots\pi$ stacking, was accomplished using Hirshfeld surface analysis, an advanced technique, providing an additional dimension for evaluating the structural stability of the molecule. These theoretical studies at the molecular scale have direct implications for the biotechnological applications of organisms at the macroscale. In this regard, investigations into the efficiency of natural systems should not only cover land-based flora but also aquatic systems.

There are many studies available in the literature related to the composition, distribution, dynamics, and interactions with environmental factors in relation to algal flora in aquatic environments (Çelik & Ongun, 2007; Tezel Ersanlı & Hasırcı, 2013; Tezel Ersanlı & Gönülol, 2014; Hasırcı Mustak & Tezel Ersanlı, 2015; Deniz & Tezel Ersanlı, 2016a; Tezel Ersanlı & Hasırcı Mustak, 2017; Tezel Ersanlı & Öztürk, 2017; Yılmaz et al., 2018; Deniz & Tezel Ersanlı, 2020a, 2020b; Solak et al., 2020; Aswathy et al., 2021; Deniz & Tezel Ersanlı, 2021a, 2021b, 2022). The results of these studies show that algae are organisms that are essential both for their nutritional value and applications in biotechnology owing to their fiber, mineral, and protein-rich nature, low-fat content, and easily digestible carbohydrate compounds

(Serrano et al., 1998; Sarı & Tüzen, 2008). It is possible due to the fact that new progress has also been made in molecular modeling and quantum chemistry studies, which have provided new insights into the success of the ability of algae to protect the environment from pollution (bioremediation). On the other hand, the use of algae in the process of bioremediation has gained new grounds during recent years. Studies have shown that such species as Spirogyra sp. and Rhizoclonium sp. could be used as bioadsorbents to remove synthetic dyes from aquatic systems (Deniz & Tezel Ersanlı, 2016b). Additionally, many efforts have been directed toward researching the biosorption capability of macroalgal species like Chaetomorpha sp., Polysiphonia sp., Ulva sp., and Cystoseira sp. for the absorption of heavy metals and pollutants (Sarı & Tüzen, 2008; Deniz & Tezel Ersanlı, 2018a, 2018b).

In conclusion, although this research focuses on the density functional theory (DFT) and Hirshfeld surface analysis of the coumarin analog obtained from *Clausena lansium*, there is also an exploration of the multidisciplinary relationship between natural products chemistry and algal biotechnology.

Materials and Methods

Molecular geometry of the title molecule (Figure 1), investigated within the framework of this research, has been determined based on the findings of Li *et al*. (2012) on the basis of the results of single crystal X-ray diffraction, and was used as an initial geometry for quantum chemistry computations. Quantum calculations related to investigation of structural and electronic parameters of the molecule in question were conducted utilizing Gaussian 03 software package (Frisch *et al*., 2004). Within quantum calculations the method of DFT was applied, where the calculations were conducted using the hybrid functional B3LYP (Becke, 1993; Lee *et al*., 1988) along with the 6-311G(d,p) basis

set accounting for correlation and exchange of electrons. Geometry optimization of the molecule was done without any restrictions in terms of its symmetry, which ensured its stability by conducting vibrational frequency analysis. The HOMO-LUMO molecular orbitals and MEPs were calculated and depicted using the GaussView 4.1.2 program (Dennington *et al*., 2007). The conformational characteristics of the molecule were studied, and its crystal structure was plotted using the Mercury CSD 2.0 software (Macrae *et al*., 2008). Also, the Hirshfeld surface was analyzed to explore the type of intermolecular forces in the crystal structure, which was examined as a 2D fingerprint plot through the CrystalExplorer 17.5 program (Turner *et al*., 2017).

Figure 1. Structure of the title compound (Li et al., 2012).

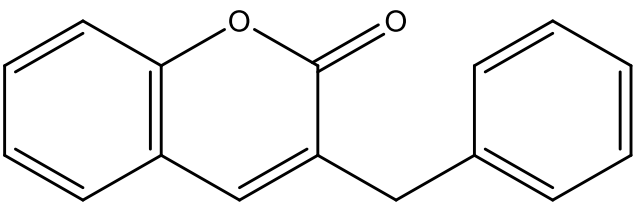

Results and Discussion

3-Benzyl-2*H*-chromen-2-one is a compound from the class of coumarin derivatives that plays an important role because of their biological and optoelectronic properties. The structural characteristics of the studied compound, known as 3-benzylchromen-2-one, have been analyzed on the basis of comparisons between the experimental and theoretical values of single crystal X-ray diffraction measurements. Experimental data have been collected on the basis of the crystal structure provided by Li *et al*. (2012). The theoretical part has been done with the help of the Gaussian 03 software with B3LYP/6-311G(d,p).

The structure of the compound comprises the usual benzopyran ring system and a benzyl substituent attached to it. When comparing the crystal structure obtained experimentally (Figure 2.a) and the optimized structure obtained theoretically (Figure 2.b), it can be seen that there is an excellent match between the two when considering various geometric parameters. The optimized structure shown in Figure 2.b was modeled using the Mercury CSD 2.0 program (Macrae *et al*., 2008).

Figure 2. (a) Crystal structure obtained experimentally and (b) optimized structure calculated at the B3LYP/6-311G(d,p) level (modeled using Mercury CSD 2.0).

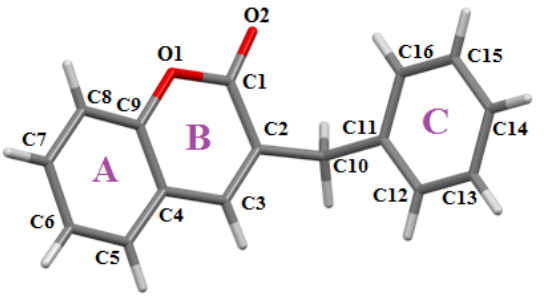

(a)

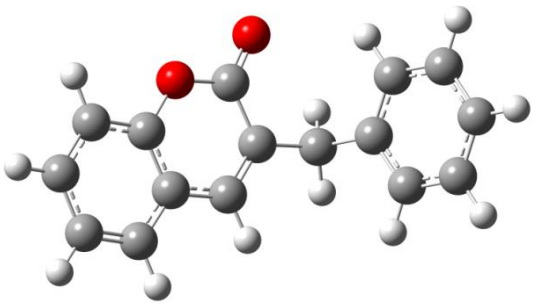

(b)

The atomic coordinates of the optimized geometry represent the lowest energy form of the compound and indicate the stability of the compound by reaching its minimum form. A comparative study of the experimental and theoretical geometrical parameters is made and shown in Table 1. While considering the bond lengths, it

is seen that the O2-C1 bond of the carbonyl group is found to be 1.2128 Å experimentally and 1.2040 Å theoretically. Likewise, the bond lengths of O1-C1 and O1-C9 bonds also correlate well. Such small errors may be considered as due to the fact that DFT calculation tends to underestimate bond lengths. When it comes to bond angles, it is seen that the value of O1-C1-O2 bond angle is found experimentally to be 116.43° and theoretically to be 117.45°. The bond angles of other atoms also show a very good correlation with experimental values. As regards the torsion angles, it may be seen that the compound shows planarity in general and the theoretical calculations also confirm it.

Table 1. Measured and calculated bond lengths (Å), bond angles (°), and torsion angles.

Bond Distances, Bond and Torsion Angles	Experimental (Li et. al., 2012)	Theoretical
O1-C1	1.3805 (13)	1.38983
O2-C1	1.2128 (13)	1.20404
O1-C9	1.3834 (13)	1.36389
C2-C10	1.5157 (14)	1.51325
C10-C11	1.5231 (14)	1.52296
C4-C9	1.3944 (16)	1.40337
O1-C1-O2	116.43 (10)	117.454
C1-O1-C9	122.30 (9)	123.086
C2-C1-O1	117.80 (9)	116.879
C2-C1-O2	125.76 (10)	125.664
C4-C9-O1	120.66 (9)	120.886
C8-C9-O1	116.75 (10)	117.671
C1-C2-C10	116.75 (9)	116.817
C2-C10-C11	111.95 (8)	113.366
C4-C9-C8	122.59 (10)	121.442
C2-C1-O1-C9	-1.63 (13)	-0.453
C4-C9-O1-C1	-1.39 (14)	-0.376
C7-C8-C9-O1	178.51 (9)	179.675
C8-C9-O1-C1	178.61 (9)	179.835

O1-C1-C2-C3	3.29 (14)	1.220
C5-C4-C9-O1	-178.70 (8)	-179.620
O1-C1-C2-C10	-175.41 (8)	-178.830
O2-C1-C2-C3	-176.32 (10)	-178.166
O2-C1-C2-C10	4.98 (15)	1.784
O2-C1-O1-C9	178.02 (9)	178.985

Properties associated with the conformation of the molecule have been discussed in detail with the help of Figure 3. This structure comprises two benzene rings (A & C) along with one pyrone ring (B). The presence of a small dihedral angle of 1.82° between rings A and B suggests that these rings exist almost in the same plane. In comparison, the angle of 72.86° between A and C rings suggests that the benzyl ring is considerably inclined towards the coumarin core. The calculated total electronic energy for the molecule is -767.5817153 Hartree, implying that the optimized structure of the molecule is stable from a thermodynamic point of view.

Figure 3. Schematic representation of dihedral angles of the inter-ring system.

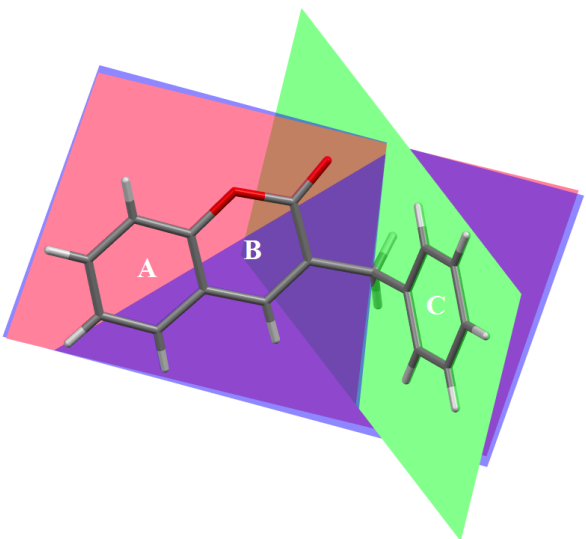

Crystal structure packing features are provided in Figure 4; this image was similarly generated by the Mercury CSD 2.0 program. The structure was found to be arranged in such a way that molecules are placed side by side along the c-axis direction within the crystal lattice. Moreover, there were weak $\pi\cdots\pi$ interactions between the aromatic rings present in the structure, with the closest distance being measured as 3.593 Å.

Figure 4. Crystal packing and π–π interaction.

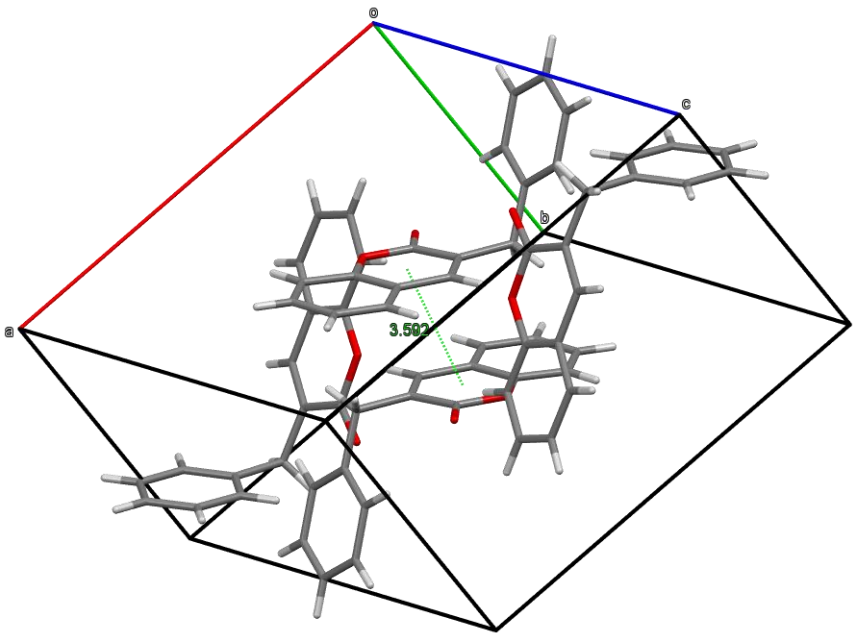

This study focuses on the analysis of the structural characteristics of a derivative of coumarin isolated from the *Clausena lansium* plant. *Clausena lansium* is abundant in coumarin derivatives and possesses numerous biological properties (Adebajo *et al*., 2009; Maneerat *et al*., 2010; Maneerat *et al*., 2012). Thus, due to the antioxidative, antimicrobial, and antitumor properties of coumarin derivatives, this kind of structural study is highly significant for clarifying the structure-activity relationship. In this

connection, a high similarity between the experimentally measured values by the X-ray method and the theoretically calculated ones at the DFT/B3LYP/6-311G(d,p) level was observed. The molecular modeling carried out with the help of the Mercury CSD 2.0 program package promoted understanding of the spatial structure of the molecule and its crystal packing. Such results both confirm the validity of theoretical techniques used and make it possible to carry out a full evaluation of structural characteristics of the investigated coumarin analogue.

HOMO, LUMO, Global Reactivity Parameters, and MEP

The electronic structure of the compound has been studied using HOMO-LUMO molecular orbitals, global reactivity parameters, and an MEP diagram. Since HOMO shows the ability of the molecule to donate electrons, while LUMO shows electron acceptance and electrophilic nature, it should be mentioned that in this case, it may be assumed that the HOMO orbital is predominantly located on the aromatic ring and conjugated system, while LUMO corresponds to the carbonyl region and its surroundings. Such analysis demonstrates the existence of intramolecular charge transfer in this molecule, while the carbonyl group plays an important role in such processes (Figure 5). The HOMO-LUMO energy gap is an essential factor as far as chemical stability and reactivity of the molecule is concerned. If there is a relatively large energy gap, then the molecule will be chemically quite stable and least reactive, and vice versa. The findings of this molecule suggest that this molecule has moderate reactivity and is prone to electrophilic and nucleophilic attacks.

Figure 5. (a) HOMO and (b) LUMO of compound.

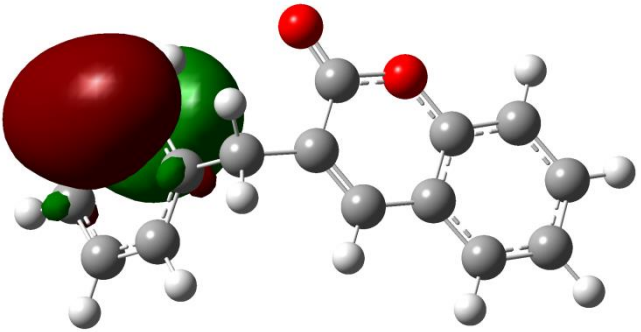

HOMO

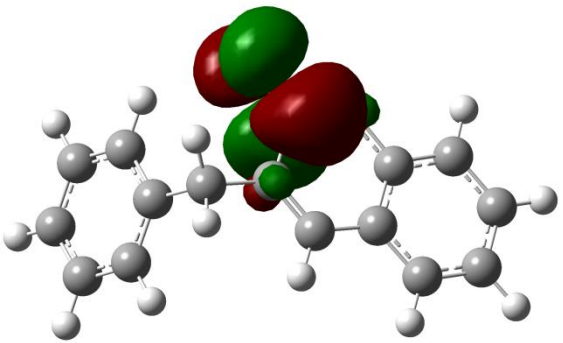

LUMO

The electronic structure of the 3-benzyl-2*H*-chromen-2-one molecule was assessed based on the energies of the molecular boundary orbitals, which were calculated with B3LYP/6-311G(d,p) theory using the DFT method. These resulted in HOMO and LUMO energies of −6.5775 eV and −2.0474 eV, respectively, and the energy difference (Δ*E*) between them being 4.5302 eV. The energy gap between the highest occupied and lowest unoccupied molecular orbitals is an essential parameter that gives insight into the stability and reactivity of the molecules. Since the bandgap was found to be quite high, the molecule under study can be considered chemically stable and kinetically highly stable. As per previous studies, the molecules that have a high energy gap are not

polarizable and stable (Miar *et al*., 2021). The chemical hardness (η) parameter was determined as 2.2651 eV. This means that the electron cloud in the molecule cannot be easily distorted. Hardness inversely correlates with the level of reactivity, and a high value of hardness corresponds to low reactivity (Alkhatib & Alsulami, 2023). Conversely, the softness (S) parameter was identified as 0.220743 eV^{-1}. This value shows that the molecule can resist any external influences, which means that the molecule has a small amount of softness. Ionization potential (I = 6.5775 eV) corresponds to the energy needed to extract one electron from the atom, and the high value of this parameter shows that the substance is not inclined to lose electrons. The value of electron affinity (A = 2.0474 eV) reflects the molecule' ability to accept electrons. The electron-donating ability of the HOMO and electron-accepting ability of the LUMO are the critical components of chemical behavior in this case.

As can be seen, the value of electronegativity (χ) amounted to 4.3125 eV, which means that the molecule has significant abilities to attract electrons. The negativity of the value of chemical potential (μ) ($\mu \approx -4.3125$ eV) confirms the thermodynamic stability and inability of the system to lose electrons. The electrophilicity index (ω) is equal to 4.1052 eV and is the characteristic of accepting electrons by the molecule in the reaction. The large value of the index is associated with a high reactivity of the molecule and a pronounced ability to interact with other substances, especially when dealing with electron-rich species. It can be assumed that the molecule has active participation in the process, especially electrophilic reaction mechanisms (Sabry *et al*., 2024). However, the 3-benzylchromen-2-one molecule has the characteristics of a stable, unreactive compound, since there is a significant energy gap between the levels of HOMO and LUMO, and the chemical hardness is also

quite high. However, it differs from others because of its ability to accept electrons due to the relatively high electrophilicity index. Such features suggest that the compound is endowed with balanced characteristics when it comes to electronic stability and the possible reactions.

MEP calculation, however, makes it possible to determine reactive areas by showing how the charge is distributed on the molecular surface. The calculated MEP ranges from -5.288×10^{-2} a.u. to $+5.288 \times 10^{-2}$ a.u. (Figure 6). Zones of negative potential are characterized by an abundance of electrons (red color), whereas positive potential zones are electron-deficient (blue color). As shown by the calculations, oxygen atoms demonstrate high negative potential value (O2: −0.0522312 a.u.; O1: −0.0352622 a.u.). That means that the indicated atoms are the parts that are most prone to be affected electrophiles. On the contrary, hydrogen atoms with positive potential (H5: 0.0257192 a.u.; H8: 0.0197924 a.u.) can act as targets for nucleophiles.

Figure 6. MEP map of compound.

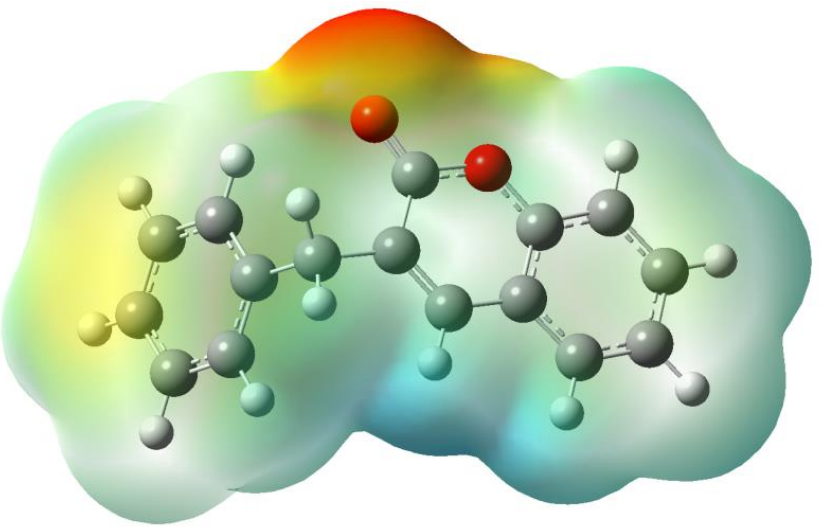

Mulliken and NPA

In this part, the distribution of the electronic charges of the 3-benzylchromen-2-one compound was studied through Mulliken and NPA analyses, which were derived from the optimized values of the compound. Even though both systems are designed for the determination of partial atomic charges, there is some difference between them.

Table 2. Mulliken and natural population analysis.

Atom	Mulliken	Natural	Atom	Mulliken	Natural
O1	-0.309292	-0.50759	**C14**	-0.080157	-0.17272
O2	-0.322707	-0.58392	**C15**	-0.085137	-0.15095
C1	0.432412	0.77570	**C16**	-0.044084	-0.17528
C2	-0.271479	-0.06876	**H3**	0.084749	0.17728
C3	0.159410	-0.11686	**H5**	0.086547	0.17300
C4	-0.174949	-0.11969	**H6**	0.093308	0.17232
C5	-0.037039	-0.13559	**H7**	0.097074	0.17099
C6	-0.084437	-0.17567	**H8**	0.105678	0.18979
C7	-0.07660	-0.13487	**H10A**	0.148735	0.21270
C8	-0.039806	-0.20269	**H10B**	0.116814	0.19235
C9	0.186292	0.35506	**H12**	0.070990	0.16506
C10	-0.163167	-0.39235	**H13**	0.084990	0.16631
C11	-0.115471	0.01090	**H14**	0.085739	0.16723
C12	-0.057757	-0.18853	**H15**	0.089364	0.16749
C13	-0.085807	-0.15723	**H16**	0.105790	0.18651

It can be noted from the data presented in Table 2 that the charge of oxygen atoms is highly negative when calculated using either method. While the Mulliken population calculation yields charges of -0.309 e for O1 and -0.323 e for O2, the charges of the atoms increase in terms of absolute value when considering natural population charge distribution (-0.508 e for O1 and -0.584 e for O2). One can thus conclude that natural population analysis is superior in terms of localizing charge distribution. It can be said that owing to the high level of electronegativity, oxygen atoms

attract electron clouds towards themselves in reactive zones of the molecule. Analyzing the data on carbon atoms, it should be noted that the C1 atom is characterized by a highly positive charge (0.432 e according to Mulliken analysis and 0.776 e according to NPA). This means that the carbon atom of the carbonyl group takes on an electrophilic nature due to the withdrawing nature of oxygen. Likewise, whereas the C9 atom is positively charged, the fact that the C10 atom is negatively charged in both analyses means that the charges within the molecule are not uniformly distributed but are located in certain parts. There exists a trend where the carbon atoms associated with the aromatic ring and benzyl group are usually negatively charged or weakly negatively charged. The reason for such charges is because of the delocalization of π electrons, an effect that is more evident in the natural population analysis. Hydrogen atoms tend to have positive charges in both forms of analyses. Whereas Mulliken charges lie between 0.07 and 0.15 e, natural charges lie between 0.16 and 0.21 e. This clearly shows that hydrogen atoms have a more electropositive nature than carbon atoms. Generally speaking, although Mulliken charges depend more on the basis set used, NPA is more reliable for obtaining accurate values that correlate better with chemical behavior. Hence, one could say that the NPA method is more trustworthy for estimating the reactivity and electrophilic/nucleophilic sites of the molecule. Such conclusions prove that the coumarin derivative under study displays specific charge distribution near the carbonyl group and oxygen atoms, thus making them potential sites for further reactions.

Hirshfeld Surface Analysis and Intermolecular Contacts

Hirshfeld surface analysis is a good technique which is commonly applied to analyze the interaction between molecules in the crystalline state quantitatively and visually. The results of the Hirshfeld surfaces and fingerprint plots analyzed here have been

calculated by means of Crystal Explorer 17.5 software (Turner *et al*., 2017). The d_{norm} parameter, which is considered to be one of the major ones during the interpretation of the results, can be calculated by the following equation:

$$d_{norm} = \frac{d_i - r_i^{vdw}}{r_i^{vdw}} + \frac{d_e - r_e^{vdw}}{r_e^{vdw}}$$

where d_i is the distance between a certain atom in the structure and the nearest atom located outside the Hirshfeld surface; while d_i is the distance between the same atom and the nearest atom inside the Hirshfeld surface. While the r_i^{vdw} and r_e^{vdw} are the van der Waals radii of the atoms present within and outside the Hirshfeld surface, respectively (Kanmazalp *et al*., 2019; Kansız & Dege, 2018). A detailed study was conducted on the interaction forces between molecules in the structure using three-dimensional Hirshfeld surfaces derived from the d_{norm} parameter (refer to Figure 7). Three-dimensional Hirshfeld surfaces provide visualization of intermolecular interactions through normalization based on the van der Waals radii of atoms, thereby differentiating between short-range interactions and long-range interactions. The three-dimensional Hirshfeld surface plotted by d_{norm} (from -0.1347 to 1.0505), as illustrated in Figure 7, facilitates intermolecular contacts analysis. The red zones present on the d_{norm} plane suggest contacts that are less than the sum of the van der Waals radii, while white zones denote nearly equivalent contacts, and the blue zones depict contacts at long ranges. The clear red spots noted in the present compound suggest that weak hydrogen bonds of the type C-H···O exist in the compound. Here, the C5-H5···O1 and C8-H8···O2 hydrogen bonding contacts are noted between adjacent molecules whose symmetry codes are (*i*) x, ½-y, ½+z and (*ii*) x, y, 1+z, respectively.

Figure 7. The representation of three-dimensional Hirshfeld surface with d_{norm}.

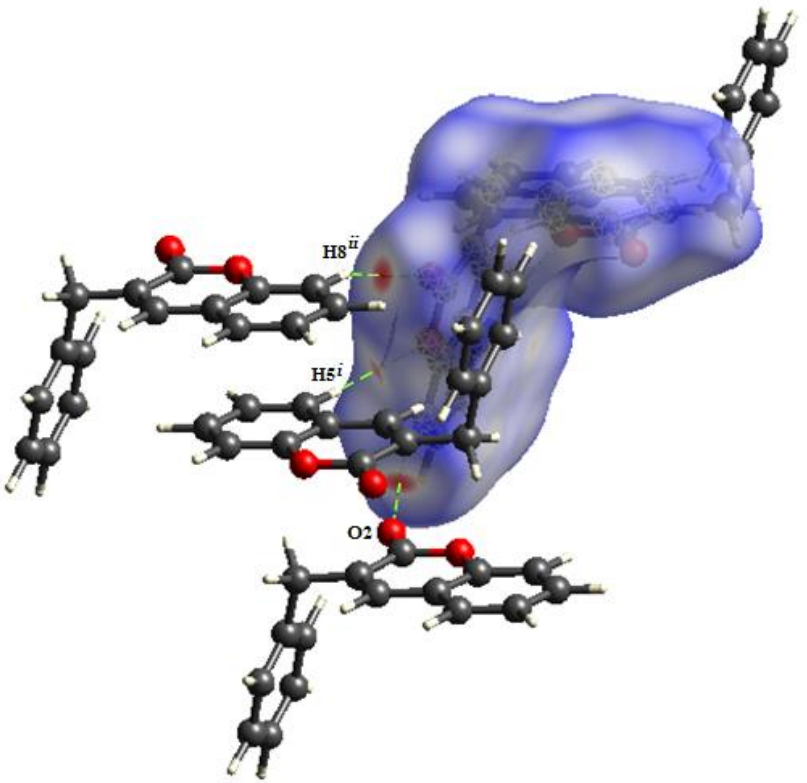

The different surface features of the Hirshfeld surface, illustrated in Figure 8 (d_{norm}, d_i, d_e, shape index, curvedness, and fragment patch), provide a deeper understanding of the interactions of the molecule with the environment. The d_i and d_e surface features show inner and outer distances of the surface, respectively; here, the range values of d_i (1.0516–2.3970 Å) and d_e (1.0521–2.3923 Å) suggest that intermolecular contacts have a wide variety of distances. On the shape index map with the range of (-1.0000, 1.0000), complementing red and blue triangle patterns particularly suggest $\pi\cdots\pi$ interactions, while curvedness map (range: -4.0000–0.4000) shows flat and curved areas of the surface, thus describing

the topology of the contact sites. Finally, the fragment patch surface feature quantitatively shows the distribution of contact sites around the molecule.

Figure 8. Hirshfeld surface analysis of the compound with d_{norm}, d_i, d_e, shape index, curvedness, and fragment patch.

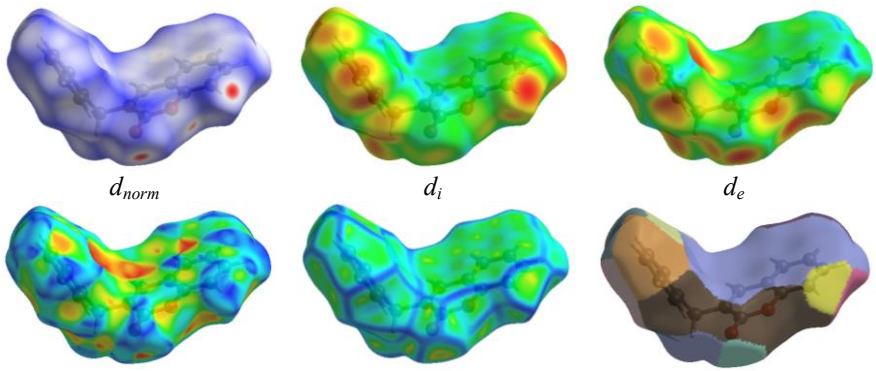

The two-dimensional fingerprint plots shown in Figure 9 demonstrate vividly how the quantitative distribution of the intermolecular contacts responsible for the Hirshfeld surface area of compound looks like. These graphs give a full insight into the nature of crystal packing, allowing us to distinguish not only the type but also the intensity of interactions leading to formation of the total surface area. Looking through the available data, it becomes evident that the strongest influence is exerted by H···H contacts (46.2%). The high percentage reveals how many hydrogen atoms are present on the molecular surface, thus indicating that the van der Waals forces are vital for stabilization of the crystal structure. Despite the fact that H···H contacts are regarded as being weak, they become crucial for the crystal packing because of their high percentage value. The second strongest contacts are represented by C···H/H···C interactions (25.9%). The third most important interaction was the O···H/H···O interaction that accounted for 17.0%. The interaction is directly linked to the C–

H···O-type weak hydrogen bonds illustrated in Figure 7. For instance, the use of carbonyl oxygen as the acceptor in the hydrogen bonds makes an immense contribution towards the stability of the crystal structure. The percentage of the contribution of the C···C interactions was estimated to be 8%. The above intermolecular contacts are usually associated with the occurrence of $\pi\cdots\pi$ interactions. Nevertheless, the relatively small percentage value shows that this kind of interactions has little significance in crystal packing. Therefore, despite the fact that there are many aromatic compounds in the structure, the $\pi\cdots\pi$ interaction cannot be the dominant type of interactions for crystal stability. The last type of interactions is represented by C···O/O···C interactions, which take up only 2.9%. These kinds of interactions are normally regarded as weak interactions between dipoles and are quite insignificant in terms of crystal packing. On the whole, the fingerprint plots of Figure 9 show that the packing of the compound is determined by ordinary van der Waals forces, namely hydrogen bonds (H···H); besides, C···H/H···C and O···H/H···O interactions provide directional contacts necessary for the stability of the crystal. It can be concluded that $\pi\cdots\pi$ and other secondary interactions have a minor contribution to it.

Figure 9. 2D-Fingerprint plots showing the contribution to the total Hirshfeld surface area of the molecule.

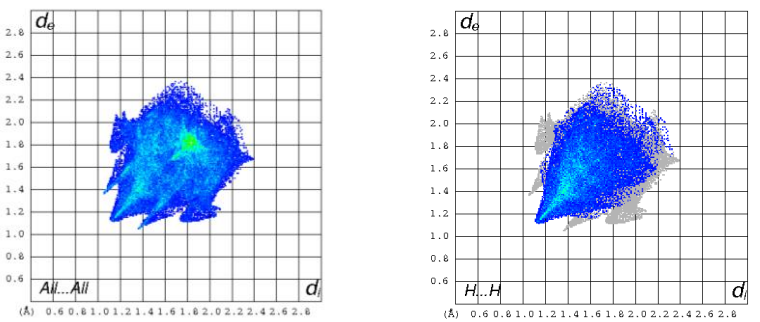

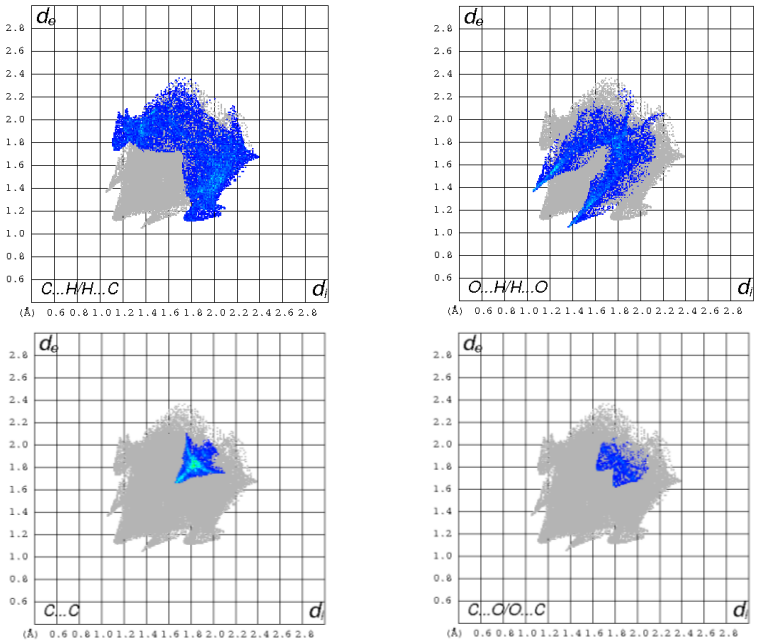

Conclusions

The structural and electronic characteristics of the 3-benzyl-2*H*-chromen-2-one compound extracted from the *Clausena lansium* plant have been thoroughly analyzed using a combination of experimental measurements carried out via single crystal X-ray diffraction and theoretical calculations based on the density functional theory. The excellent agreement between the structural parameters obtained from geometry optimization at the B3LYP/6-311G(d,p) level and experimental data clearly suggests that the applied theoretical approach can be effectively utilized to accurately characterize the molecular structure of the target compound. The minor discrepancies in the bond lengths, bond angles, and torsional angles are reasonable, taking into account the nature of the DFT method. The analysis of the electronic structure shows that the molecule displays a high HOMO-LUMO energy gap, which indicates its kinetic stability and low reactivity. Low

values of chemical hardness and high values of softness provide evidence of the molecule's resistance to external effects. At the same time, the electrophilicity index, which is available at a certain value, speaks of the presence of active sites of the molecule that can react with electron-rich reagents. Studies conducted using the method of MEP show that the zones of negative potential are located primarily on oxygen atoms, which indicates their sensitivity to electrophiles. At the same time, positive values of potential at the sites of hydrogen atoms show that these areas are prone to nucleophilic reactions. Analysis using methods of Mulliken and NPA has shown that there is an uneven distribution of the charge in the molecule and that oxygen atoms have a negative charge. The fact that NPA provides more reliable results than Mulliken calculations made it possible to study intramolecular transfers more accurately. Hirshfeld analysis of surfaces and fingerprint plots allow us to study the properties of intermolecular interactions. From the results of the analyses performed, it is observed that there are van der Waals forces such as H···H interactions (46.2%) that mainly determine the nature of the crystal packing. Other interactions like C···H/H···C (25.9%) and O···H/H···O (17.0%) contacts also contribute to the stabilization of the crystal packing. It was also observed that weak C–H···O hydrogen bonds are essential in determining the structure of the crystals. Finally, from the study, it is clear that $\pi\cdots\pi$ interactions such as those involving C···C (8%) and others such as the C···O/O···C contact are minor contributors to the crystal packing of the compound.

To sum up, the current research explains the structure features of the 3-benzyl-2*H*-chromen-2-one molecule in terms of its molecular and crystalline structure. Thus, the results obtained can be considered a contribution to the analysis of the structural properties of coumarin compounds and may become an excellent scientific basis for future research related to this topic.

References

Adebajo, A. C., Iwalewa, E. O., Obuotor, E. M., Ibikunle, G. F., Omisore, N. O., Adewunmi, C. O., Obaparusi, O. O., Klaes, M., Adetogun, G. E., Schmidt, T. J., & Verspohl, E. J. (2009). Pharmacological properties of the extract and some isolated compounds of *Clausena lansium* stem bark: anti-trichomonal, antidiabetic, anti-inflammatory, hepatoprotective and antioxidant effects. *Journal of ethnopharmacology*, *122*(1), 10-19. https://doi.org/10.1016/j.jep.2008.11.015

Alkhatib, F. M., & Alsulami, H. M. (2023). Synthesis, characterization, DFT calculations and biological activity of new Schiff base complexes. *Heliyon*, *9*(8), e18988. https://doi.org/10.1016/j.heliyon.2023.e18988

Aswathy, U., Pandey, A. K., Sharma, P., Sreekumar, N., & Kumar, S. (2021). Emerging industrial applications of microalgae: Challenges and future perspectives. *Systems Microbiology and Biomanufacturing*, *1*(4), 411-431. https://doi.org/10.1007/s43393-021-00038-8

Becke, A. D. (1993). Density-functional thermochemistry. III. The role of exact exchange. *The Journal of Chemical Physics*, *98*(7), 5648-5652. https://doi.org/10.1063/1.464913

Çelik, K., & Ongun, T. (2007). The influence of certain physical and chemical variables on the seasonal dynamics of phytoplankton assemblages of a source inlet and the outlet of the shallow hypertrophic Lake Manyas, Turkey. *Turkish Journal of Botany*, *31*(6), 485-493.

Deniz, F., & Tezel Ersanlı, E. (2016a). Simultaneous bioremoval of two unsafe dyes from aqueous solution using a novel green composite biosorbent. *Microchemical Journal*, *128*, 312-319. https://doi:10.1016/j.microc.2016.05.012

Deniz, F., & Tezel Ersanlı, E. (2016b). Removal of colorant from simulated wastewater by phyco-composite material: Equilibrium, kinetic and mechanism studies in a lab-scale application. *Journal of Molecular Liquids*, *220*, 120-128. https://doi.org/10.1016/j.molliq.2016.04.081

Deniz, F., & Tezel Ersanlı, E. (2018a). An ecofriendly approach for bioremediation of contaminated water environment: Potential contribution of a coastal seaweed community to environmental improvement. *International Journal of Phytoremediation*, *20*(3), 256-263. https://doi.org/10.1080/15226514.2017.1374335

Deniz, F., & Tezel Ersanlı, E. (2018b). A natural macroalgae consortium for biosorption of copper from aqueous solution: Optimization, modeling and design studies. *International Journal of Phytoremediation*, *20*(4), 362-368. https://doi.org/10.1080/15226514.2017.1393387

Deniz, F., & Tezel Ersanlı, E. (2020a). An effectual biosorbent substance for removal of manganese ions from aquatic environment: A promising environmental remediation study with activated coastal waste of *Zostera marina* plant. *BioMed Research International*, *2020*(1), 7806154, 1-8. https://doi.org/10.1155/2020/7806154

Deniz, F., & Tezel Ersanlı, E. (2020b). A low-cost and eco-friendly biosorbent material for effective synthetic dye removal from aquatic environment: Characterization, optimization, kinetic, isotherm and thermodynamic studies. *International Journal of Phytoremediation*, *22*(4), 353-362. https://doi.org/10.1080/15226514.2019.1663485

Deniz, F., & Tezel Ersanli, E. (2021a). A renewable biosorbent material for green decontamination of heavy metal

pollution from aquatic medium: A case study on manganese removal. *International Journal of Phytoremediation*, *23*(3), 231-237. https://doi.org/10.1080/15226514.2020.1807905

Deniz, F., & Tezel Ersanli, E. (2021b). Purification of malachite green as a model biocidal agent from aqueous system by using a natural widespread coastal biowaste (*Zostera marina*). *International Journal of Phytoremediation*, *23*(7), 772-779. https://doi.org/10.1080/15226514.2020.1857684

Deniz, F., & Tezel Ersanlı, E. (2022). A novel biowaste-based biosorbent material for effective purification of methylene blue from water environment. *International Journal of Phytoremediation*, *24*(12), 1243-1250. https://doi.org/10.1080/15226514.2021.2025039

Dennington, R., Keith, T., & Millam, J. (2007). *GaussView* (Version 4.1.2). Semichem Inc.

Frisch, M. J., Trucks, G. W., Schlegel, H. B., Scuseria, G. E., Robb, M. A., Cheeseman, J. R., Montgomery, J. A., Jr., Vreven, T., Kudin, K. N., Burant, J. C., Millam, J. M., Iyengar, S. S., Tomasi, J., Barone, V., Mennucci, B., Cossi, M., Scalmani, G., Rega, N., Petersson, G. A., Nakatsuji, H., Hada, M., Ehara, M., Toyota, K., Fukuda, R., Hasegawa, J., Ishida, M., Nakajima, T., Honda, Y., Kitao, O., Nakai, H., Klene, M., Li, X., Knox, J. E., Hratchian, H. P., Cross, J. B., Bakken, V., Adamo, C., Jaramillo, J., Gomperts, R., Stratmann, R. E., Yazyev, O., Austin, A. J., Cammi, R., Pomelli, C., Ochterski, J. W., Ayala, P. Y., Morokuma, K., Voth, G. A., Salvador, P., Dannenberg, J. J., Zakrzewski, V. G., Dapprich, S., Daniels, A. D., Strain, M. C., Farkas, O., Malick, D. K., Rabuck, A. D., Raghavachari, K., Foresman, J. B., Ortiz, J. V., Cui, Q., Baboul, A. G., Clifford, S., Cioslowski, J., Stefanov, B. B., Liu, G., Liashenko, A., Piskorz, P., Komaromi, I., Martin, R. L., Fox, D. J., Keith, T., Al-Laham, M. A., Peng, C. Y., Nanayakkara, A.,

Challacombe, M., Gill, P. M. W., Johnson, B., Chen, W., Wong, M. W., Gonzalez, C., & Pople, J. A. (2004). *Gaussian 03*, Revision C.02. Gaussian, Inc.

Hasırcı Mustak, S., & Tezel Ersanlı, E. (2015). Spatial and temporal characterization of the physicochemical parameters and phytoplankton assemblages in Dodurga Reservoir (Sinop, Turkey). *Turkish Journal of Botany*, *39*(3), 547-554. https://doi.org/10.3906/bot-1407-32

Kanmazalp, S. D., Macit, M., & Dege, N. (2019). Hirshfeld surface, crystal structure and spectroscopic characterization of (*E*)-4-(diethylamino)-2-((4-phenoxyphenylimino) methyl) phenol with DFT studies. *Journal of Molecular Structure*, *1179*, 181-91. https://doi.org/10.1016/j.molstruc.2018.11.001

Kansız, S., & Dege, N. (2018). Synthesis, crystallographic structure, DFT calculations and Hirshfeld surface analysis of a fumarate bridged Co(II) coordination polymer. *Journal of Molecular Structure*, 2018, *1173*, 42-51. https://doi.org/10.1016/j.molstruc.2018.06.071

Lee, C. T., Yang, W. T., & Parr, R. G. (1988). Development of the Colle-Salvetti correlation-energy formula into a functional of the electron density. *Physical Review B*, *37*, 785-789. https://doi.org/10.1103/PhysRevB.37.785

Li, G. Q., Li, Y. L., Jiang, T., Jiang, R. W., & Wang, G. C. (2012). 3-Benzyl-2*H*-chromen-2-one. *Acta Crystallographica Section E Structure Reports Online*, *68*(5), o1504. https://doi.org/10.1107/S1600536812014298

Macrae, C.F., Bruno, I.J., Chisholm, J.A., Edgington, P.R., McCabe, P., & Pidcock, E. (2008). *Mercury CSD 2.0* - New features for the visualization and investigation of crystal structures.

Journal of Applied Crystallography, 41, 466-470. https://doi.org/10.1107/S0021889807067908

Maneerat, W., Prawat, U., Saewanc, N., & Laphookhieo, S., (2010). New Coumarins from *Clausena lansium* Twigs. *Journal of the Brazilian Chemical Society*, *21*(4), 665-668. https://dx.doi.org/10.1590/S0103-50532010000400012

Maneerat, W., Ritthiwigrom, T., Cheenpracha, S., Laphookieo, S., (2012). Carbazole alkaloids and coumarins from *Clausena lansium* roots. *Phytochemistry Letters*, *5*(1), 26-28. https://doi.org/10.1016/j.phytol.2011.08.013

Miar, M., Shiroudi, A., Pourshamsian, K., Oliaey, A. R., & Hatamjafari, F. (2021). Theoretical investigations on the HOMO–LUMO gap and global reactivity descriptor studies, natural bond orbital, and nucleus-independent chemical shifts analyses of 3-phenylbenzo[*d*]thiazole-2(3*H*)-imine and its *para*-substituted derivatives: solvent and substituent effects. *Journal of Chemical Research*, 45, 147-158. https://doi.org/10.1177/1747519820932091

Sabry, N. M., Badry, R., Abdel-Gawad, F. K., Elhaes, H., & Medhat, A. İ. (2024). Electronic structure, global reactivity descriptors and nonlinear optical properties of glycine interacted with ZnO, MgO and CaO for bacterial detection. *Scientific Reports, 14*, 22801. https://doi.org/10.1038/s41598-024-72846-6

Sarı, A., & Tüzen, M. (2008). Biosorption of Pb(II) and Cd(II) from aqueous solution using green alga (*Ulva lactuca*) biomass. *Journal of Hazardous Materials*, *152*(1), 302-308. https://doi.org/10.1016/j.jhazmat.2007.06.097

Serrano, A., Palacios, C., Roy, G., Cespón, C., Villar, M. L., Nocito, M., & González-Porqué, P. (1998). Derivatives of gallic acid induce apoptosis in tumoral cell lines and inhibit lymphocyte

proliferation. *Archives of Biochemistry and Biophysics*, *350*(1), 49-54. https://doi.org/10.1006/abbi.1997.0474

Solak, C. N., Peszek, Ł., Yilmaz, E., Ergül, H. A., Kayal, M., Ekmekçi, F., Várbíró, G., Yüce, A. M., Canli, O., Binici, M. S., & Ács, É. (2020). Use of diatoms in monitoring the Sakarya River Basin, Turkey. *Water*, *12*(3), 703. https://doi.org/10.3390/w12030703

Tezel Ersanlı, E., & Gönülol, A. (2014). Phytoplankton dynamics and some physicochemical variables in Cakmak Reservoir, Samsun, Turkey. *MANAS Journal of Agriculture and Life Sciences*, *4*(1), 17-25.

Tezel Ersanlı, E., & Hasırcı, S. (2013). The relationship between environmental variables and the vertical and horizontal assemblages of phytoplankton in Erfelek Reservoir in Sinop, Turkey. *Turkish Journal of Botany*, *37*(4), 715-726. https://doi.org/10.3906/bot-1207-21

Tezel Ersanlı, E., & Hasırcı Mustak, S. (2017). Distribution dynamics of vegetative cells and cyst of *Ceratium hirundinella* in two reservoirs, Turkey. Süleyman Demirel University *Journal of Natural and Applied Sciences*, *21*(1), 247-253. https://doi.org/10.19113/sdufbed.99878

Tezel Ersanlı, E., & Öztürk, R. (2017). Ecological and statistical evaluation of algal flora and water quality of Karasu Stream. *KSU Journal of Natural Sciences*, *20*(3), 193-200. https://doi.org/10.18016/ksudobil.264177

Turner, M. J., McKinnon, J. J., Wolff, S. K., Grimwood, D. J., Spackman, P. R., Jayatilaka, D., & Spackman, M. A. (2017). *CrystalExplorer17 (Version 17.5)*. University of Western Australia.

Yılmaz, N., Yardımcı, C. H., Elhag, M., & Dumitrache, C. A. (2018). Phytoplankton composition and water quality of Kamil Abduş Lagoon (Tuzla Lake), Istanbul-Turkey. *Water*, *10*(5), 603. https://doi.org/10.3390/w10050603

BÖLÜM 0

STRUCTURAL AND ELECTRONIC PROPERTIES OF NATURALLY EXTRACTED (*S*)-8-HYDROXYCHROMENONE

CEM CÜNEYT ERSANLI[1]

Introduction

In addition to having vital significance in terms of molecular biology, the biological molecules' study in nature is equally critical from the perspective of biotechnology and medicine. There have been a number of exhaustive investigations on the biochemical makeup of algae flora in aquatic environments, as well as their dynamics and interaction with environmental factors (Çelik & Ongun, 2007; Tezel Ersanlı & Hasırcı, 2013; Tezel Ersanlı & Gönülol, 2014; Hasırcı Mustak & Tezel Ersanlı, 2015; Deniz & Tezel Ersanlı, 2016a; Tezel Ersanlı & Hasırcı Mustak, 2017; Tezel Ersanlı & Öztürk, 2017; Yılmaz *et al*., 2018; Deniz & Tezel Ersanlı, 2020a, 2020b; Solak *et al*., 2020; Aswathy *et al*., 2021; Deniz & Tezel Ersanlı, 2021a, 2021b, 2022). These findings indicate that algae are significant organisms nutritionally and technologically because of their rich fiber, minerals, and proteins,

[1] Prof. Dr., Sinop University, Faculty of Arts and Science, Department of Physics, Sinop/Turkey, Orcid: 0000-0002-8113-5091, ccersanli@sinop.edu.tr, ccersanli@gmail.com

low fats, and easily digestible carbohydrates (Serrano *et al*., 1998; Sarı & Tüzen, 2008; Li *et al*., 2015). On the other hand, the utilization of algae as bioremediation tools has also witnessed considerable advancements in recent times. The usage of certain algae types including *Spirogyra* sp. and *Rhizoclonium* sp. as biological adsorbents for cleaning synthetic dyes from aquatic ecosystems has already been proven (Deniz & Tezel Ersanlı, 2016b). Moreover, the biosorption capabilities of different macroalgae such as *Chaetomorpha* sp., *Polysiphonia* sp., *Ulva* sp., and *Cystoseira* sp. have also gained extensive consideration due to their capability to eliminate heavy metals and pollutants through biosorption (Sarı & Tüzen, 2008; Deniz & Tezel Ersanlı, 2018a, 2018b). The above findings reveal that algae not only constitute ecological but also biological resources concerning sustainable environments. Moreover, microorganisms, especially fungi including the genus Penicillium, play a critical role in biotechnology because they have the capacity of producing biological metabolites and natural products (Pitt *et al*., 2000; Frisvad & Samson, 2004; Raja *et al*., 2017). Natural compounds isolated from the fungus Penicillium sp. play an essential part in the production of biological compounds like pharmaceutical drugs, enzymes, and antibiotics. For instance, (*S*)-8-hydroxy-3-(2-hydroxypropyl)-6-methoxy-2*H*-chromen-2-one obtained from *Penicillium* sp. plays an important role in natural products research based on structural and biochemical analyses of the molecule. Within this scenario, the study of natural products at the molecular level plays a pivotal role in gaining insights into the structural and electronic nature of the molecule, apart from determining its ability to adapt to the environment and its biotechnological applications. Theoretical methods such as the highest occupied molecular orbital (HOMO)-lowest unoccupied molecular orbital (LUMO) analysis based on density functional theory (DFT), chemical reactivity, molecular electrostatic potential (MEP) analysis, Mulliken

population analysis, natural population analysis (NPA), and Hirshfeld surfaces (HSs) can prove useful in elucidating the reactivity and molecular interactions of *Penicillium* sp. compounds.

The main aim of the current research is to explore the compound named Berkecoumarin, isolated from *Penicillium* sp., whose systematic name is (*S*)-8-hydroxy-3-(2-hydroxypropyl)-6-methoxy-2*H*-chromen-2-one (Decato *et al*., 2024), based on a combination of experiment and theory (Figure 1). With this aim, the structure of Berkecoumarin derived from X-ray crystallography data (Decato *et al*., 2024) was compared with the output of geometry optimization carried out on the basis of the DFT method at the B3LYP 6-311(d,p) level; Moreover, charge distribution was studied using Mulliken and NPA techniques; chemical reactivity was studied using the frontier orbitals of HOMO-LUMO; the electrostatic distribution was studied using the maps of the MEP; and intramolecular interaction was studied in depth using the HS approach. This analysis focuses on providing a more thorough insight into not only the structural characteristics of Berkecoumarin but also into its chemical properties and biological activities.

Materials and Methods

The present experiment was performed with the help of the X-ray diffraction technique, while the structure of the compound under investigation has been deposited in the CCDC database by the number: 2337933; 2331641 (Decato *et al*., 2024), whereby the theoretical studies were performed with the help of DFT calculations with B3LYP hybrid functional.

Figure 1. The chemical structure of berkecoumarin.

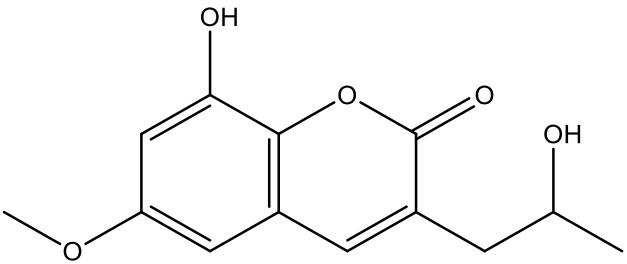

Experimental geometry of the berkecoumarin molecule was derived from the work of Decato *et al*. (2024), published in X-ray diffraction experiments on a single crystal of the compound, and used as an input geometry for theoretical calculations. All quantum chemical calculations of the studied molecule's structural and electronic properties were carried out using the Gaussian 03 program package (Frisch *et al*., 2004). For this purpose, DFT calculations were utilized, and the basis set of 6-311(d,p) along with the B3LYP hybrid functional was selected (Lee *et al*., 1988; Becke, 1993). Visualization of optimized molecular geometries, boundary molecular orbitals, and electrostatic potential surfaces was done with the aid of GaussView 4.1.2 software (Dennington *et al*., 2007). Furthermore, HS analysis was carried out to determine the type of interactions between molecules within the crystal lattice, and the results were plotted using the CrystalExplorer 17.5 software (Turner *et al*., 2017).

Results and Discussion

Berkecoumarin ($C_{13}H_{14}O_5$) is an example of a natural compound having a substitution of 3-alkyl-6,8-dioxy, which is very unusual for compounds of the coumarin family. The compound has a wide conjugation system as it consists of hydroxyl and methoxy groups along with the chromone skeleton. Experimental evidence showed that the absolute configuration of the compound is *S*-

enantiomer; this is seen as an important criterion from a biological point of view.

Figure 2. (a) Experimental structure and (b) optimized structure of the compound.

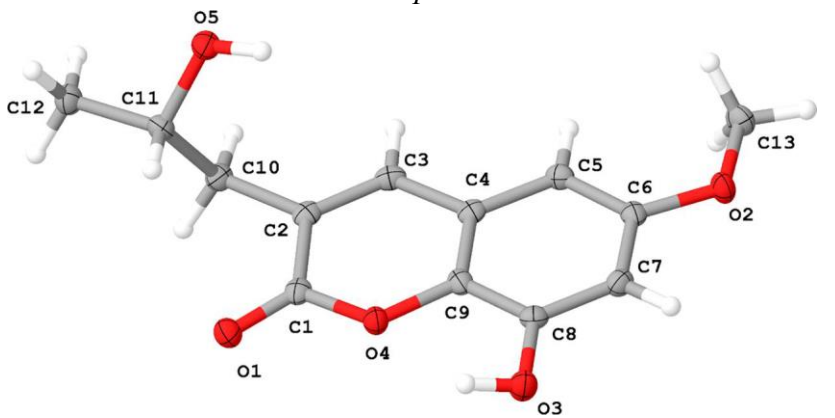

(a)

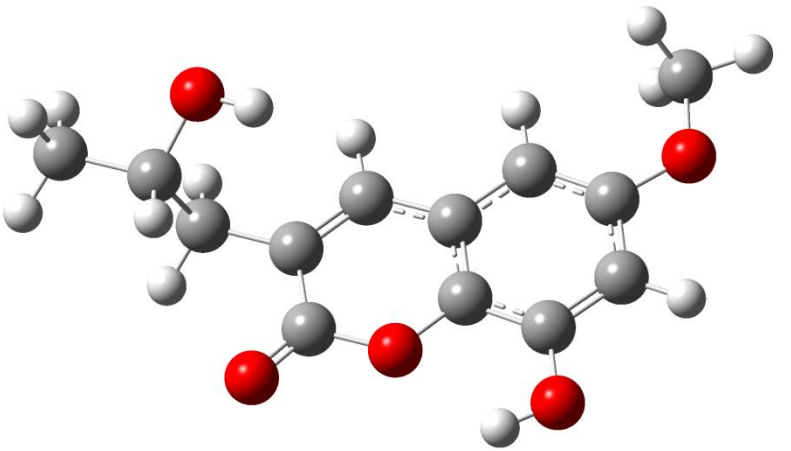

(b)

The experimental results obtained for single crystal X-ray diffraction and theoretical calculations carried out for geometric parameters based on the Gaussian 03 software employing the DFT/B3LYP/6-311(d,p) basis set are shown in Table 1 and Figure 2. When the bond lengths shown in Table 1 are carefully

considered, it is seen that there is a high degree of correlation between experimental and theoretical results. The O1–C1 bond length of the carbonyl group was found to be 1.217 Å from experiments and 1.203 Å from theoretical calculations. Such findings illustrate that the current level of theory properly accounts for the nature of the carbonyl bond (Frisch et al., 2004). In addition, it should be noted that according to previous DFT studies conducted on similar coumarin analogues, the typical value of the C=O bond length equals 1.20-1.22 Å. As it can be seen, the bond lengths of the current system O2-C6 and O4-C1 (ethereal and ester-like nature) also perfectly agree with such experimental findings. This is because the bond lengths are critical parameters that can be affected by the distribution of electrons and resonance; it is for this reason that the agreement between experimental and theoretical values makes it credible (Kumar *et al*., 2020). The same goes for the bond length values for O3-C8 and O5-C11 bonds which have no considerable discrepancy from coumarins and their analogues reported in the literature. Bond angle assessment reveals high levels of agreement between experimental and theoretical values for O1-C1-O4, O1-C1-C2, and O4-C1-C2 angles especially in the vicinity of the carbonyl carbon atom. This finding proves that the sp^2-hybridized atoms in the molecule have been accurately described. Also, the O2-C6-C7 and O3-C8-C9 angles in the aromatic system have been accurately estimated theoretically. According to scientific literature, such angles in aromatic and heteroaromatic systems lie in the range of 118-122°, and the obtained results are in line with it. After studying the dihedral angles, it becomes evident that the Berkecoumarin molecule has a flat geometry. For example, the O2-C6-C7-C8 and O3-C8-C9-C4 dihedral angles amount to nearly ±180°, which means that π-conjugation has been maintained (Kumar *et al*., 2020). This is vital when it comes to the electronic structure and biological activity of the studied molecule. According to scientific literature, the planarity of coumarin derivatives is

important, especially in their interactions with the binding sites of enzymes. Nonetheless, there was a relatively greater difference between the experimental (67.3°) and theoretical (61.1°) values of the C2-C10-C11-O5 dihedral angle. Such a discrepancy arose because of the conformational mobility of the side chain. Whereas intermolecular forces in the crystalline lattice, such as hydrogen bonding and van der Waals forces, could affect such dihedral angles, density functional theory computations executed in the gas phase could fail to capture such influences (Frisch *et al*., 2004). In a similar vein, comparable differences have been noted in other studies on coumarin derivatives with side chains analogous to those present in the target compound. The main contributors to such differences in experimental and theoretical values are crystal packing, thermal effects, and the environment. However, the overall consistency between theoretical and experimental values indicates that the B3LYP/6-311(d,p) level of theory could be used as a suitable approach for analyzing the structure of natural products like Berkecoumarin. Indeed, the results suggest that density functional theory is an efficient technique for analyzing conjugated systems like coumarin derivatives. Moreover, the planarity of the molecule and its conjugated π-system are structural parameters that correlate well with biological activities in the literature.

Table 1. Selected ground-state geometrical parameters of I: experimental and optimized values. Bond lengths (Å) and bond angles (°) are given together with their standard deviations in parentheses.

Bond Distances, Bond and Torsion Angles	**Experimental (Decato *et al*., 2024)**	**Theoretical**
O1-C1	1.217 (3)	1.20340
O2-C6	1.369 (3)	1.36137
O2-C13	1.428 (3)	1.42115

O3-C8	1.358 (3)	1.35472
O4-C1	1.369 (3)	1.39267
O4-C9	1.378 (3)	1.37099
O5-C11	1.434 (3)	1.42980
C6-O2-C13	116.4 (2)	118.413
C1-O4-C9	122.0 (2)	122.554
O1-C1-O4	116.5 (2)	117.694
O1-C1-C2	125.9 (2)	126.026
O4-C1-C2	117.6 (2)	116.281
O4-C9-C4	121.7 (2)	122.302
O4-C9-C8	116.6 (2)	116.251
O5-C11-C10	110.3 (2)	110.855
O5-C11-C12	106.5 (2)	106.648
O2-C6-C5	124.9 (2)	124.651
O2-C6-C7	114.7 (2)	114.707
O3-C8-C7	119.9 (2)	120.374
O3-C8-C9	122.0 (2)	120.927
O2-C6-C7-C8	-178.5 (2)	-179.983
O3-C8-C9-C4	179.7 (2)	-179.914
C1-O4-C9-C8	179.6 (2)	179.517
C2-C10-C11-O5	67.3 (3)	61.139
C4-C5-C6-O2	178.5 (2)	179.985
C5-C4-C9-O4	-177.5 (2)	-179.914
C6-C7-C8-O3	178.7 (2)	179.991
C13-O2-C6-C7	177.5 (2)	179.826

HOMO, LUMO, Global Reactivity Parameters, and MEP

On analyzing the distribution of the HOMO and LUMO orbitals, it becomes evident that the HOMO is mainly distributed over the chromone ring structure and specifically over the oxygen atoms present near the hydroxyl and methoxy groups. This suggests that these parts of the molecule are rich in electrons and hence are possible active sites against electrophile attack. On the other hand, it was established that the LUMO orbital is distributed over the

entire conjugated system and is localized specifically on the carbonyl group (Geerlings *et al*., 2003; Roy *et al*., 2015).

Figure 3. (a) HOMO and (b) LUMO of compound.

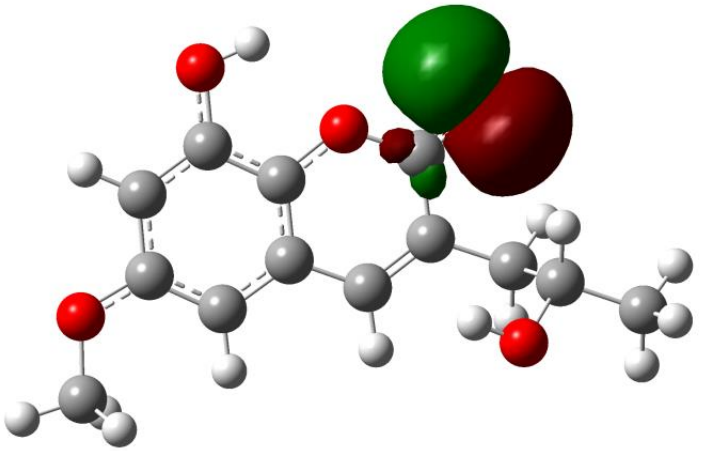

HOMO

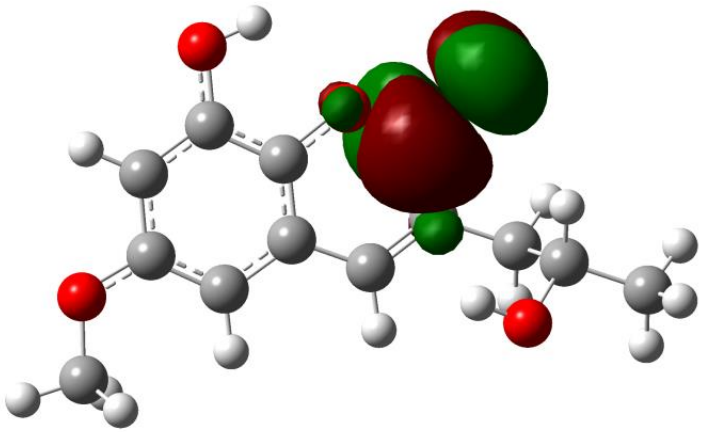

LUMO

The energy difference (ΔE = 4.0564 eV) obtained from the calculated E_{HOMO} (−6.2102 eV) and E_{LUMO} (−2.1538 eV) values indicates that the molecule possesses high electronic stability (Figure 3). The wide HOMO–LUMO energy gap is associated with low polarizability and limited chemical reactivity, indicating that

the molecule exhibits a structure resistant to external influences (Parr & Yang, 1989; Domingo *et al*., 2016). Global reactivity parameters quantitatively support this finding. The electronegativity (χ = 4.1820 eV), derived from the ionization energy (I) and electron affinity (A) values, indicates that the molecule's electron-withdrawing tendency is balanced. The high chemical hardness (η = 2.0282 eV) value indicates that the system is resistant to charge transfer, while the low softness (S = 0.2465 eV^{-1}) value confirms that the molecule has limited reactivity. According to the values of the electrophilic index (ω = 4.3115 eV), one can assume the presence of an adequate electrophilic nature of the compound and its ability to react with nucleophiles under appropriate conditions (Chakraborty *et al*., 2021; according to the Conceptual DFT approach). If all the results obtained are combined into a single picture, then the localization of the HOMO shows electron-donor areas in the structure of the compound, whereas the spatial arrangement of the LUMO determines the areas of electronic acceptors. The quantitative data of global reactivity characteristics prove the above conclusions made regarding the molecular orbitals. In this regard, Berkecoumarin is described as a highly conjugated and electronically stable reactive system. These features imply that the substance might provide some benefits in regard to selective bonding and forming a stable complex when interacting with biological target molecules (Domingo *et al*., 2016).

The MEP values are in the range of -4.722×10^{-2} a.u. to $+4.722 \times 10^{-2}$ a.u. (Figure 4). Such values reflect a unique charge distribution existing within the molecule and prove the substantial participation of electrostatic interaction in the process of molecular recognition. The negative electrostatic potential zones (in red) tend to be located mostly near oxygen atoms, whereas the positive electrostatic potential zones (in blue) appear near hydrogen atoms (Murray & Politzer, 2017).

Figure 4. MEP map of compound.

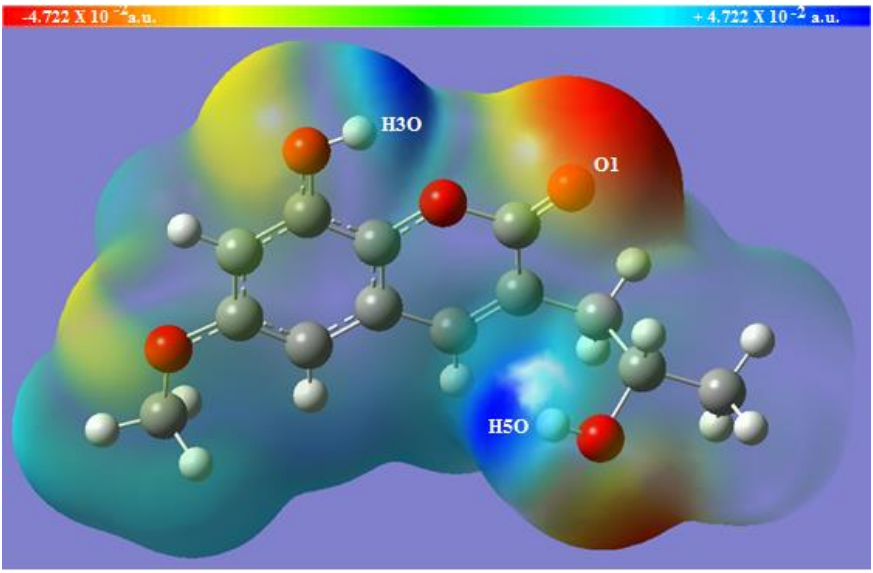

In particular, it has been established that the O1 atom (-0.0463747 a.u.), as well as the O5 atom (-0.0414160 a.u.), have the maximum negative potential. The mentioned data suggest that the discussed oxygen atoms have electron excesses and can easily interact with the substances having electrophilic behavior. Furthermore, the discussed atoms are important in relation to their ability to create hydrogen bonds. At the same time, the H5O atom (+0.0415928 a.u.) and H3O atom (+0.0443541 a.u.) are associated with hydroxyl groups, thus being positively charged and serving as donors of hydrogen bonds. This suggests that the molecule may play an active role in intermolecular interactions (Politzer *et al*., 2013). From the MEP of Berkecoumarin, it can be seen that this molecule has a polar nature, and there is an intramolecular charge transfer from the oxygen atoms to the π-conjugated system. Even though the negative and positive regions are evenly distributed in the molecule, it can be stated that the compound has a structure that is compatible with nucleophilic as well as electrophilic reactions.

Finally, it can be stated that reactive sites in the compound were determined through MEP calculations, and oxygen atoms can be considered as electrophilic targets whereas hydroxyl hydrogen atoms as hydrogen bond donors. These electrostatic properties provide important insights into the molecule's binding behavior in biological systems and molecular recognition mechanisms.

Mulliken and NPA

The results of Mulliken and NPA analysis offer significant details regarding the electronic configuration and reactive character of the molecule. As seen from the above data (Table 2), all oxygen atoms (O1-O5) are characterized by a significantly negative charge. In addition, it can be noted that the O5 atom (-0.76482 e, NPA) and O3 atom (-0.64609 e, NPA) are considered the most nucleophilic elements of the compound. In addition, the high value of the negative charge demonstrates that oxygen atoms show a high ability to react with electrophiles and also possess specific hydrogen-bond-acceptor properties (Lu & Chen, 2012; Politzer *et al*., 2013). All carbon atoms (C1-C6) within the aromatic ring show various charge values depending on their chemical environment. In particular, the very high positive charge on the C1 atom (0.76708 e, NPA) points to significant electron deficiency in the mentioned atom; hence the area becomes prone to electrophilic attack. On the contrary, other aromatic or aliphatic carbon atoms having either low positive charges or even negative charges result in heterogeneity of the reactive properties of the compound. Such a scenario accounts for reactivity differences in specific parts of the molecule (Roy *et al*., 2015). As for the charges on hydrogen atoms, one notices the very high positive charge on hydrogen atoms H3O (0.46334 e, NPA) and H5O (0.45417 e, NPA). This effect makes the hydrogen atoms in the molecule more prone to be hydrogen bond donors and improves their ability to interact with other molecules. In this regard, it is known that such acidic protons

significantly contribute to hydrogen bond formation and stability (Murray & Politzer, 2017). A comparison of Mulliken and NPA charges reveals that the latter produces more clear-cut charge distributions. This is because it is known that due to the strong dependence of Mulliken charges on the basis set used, they are often more scattered and method-dependent (Lu & Chen, 2012; Domingo *et al*., 2016). Hence, NPA charge distribution provides more reliable data concerning the molecular reactivity. In turn, the charge distribution analysis allows us not only to reveal the reactive sites of the molecule but also predict the hydrogen bonding and other electrostatic interaction patterns. Considering all these findings together with HOMO-LUMO orbital calculations and MEP outcomes makes it possible to get a more comprehensive picture of the electronic structure of the molecule. In addition, considering the results of the analysis of the charge distribution along with the concepts of frontier orbitals allows one to make more complete conclusions concerning the reactivity properties and bonding tendencies of a given molecule (Geerlings *et al*., 2003; Domingo *et al*., 2016). Therefore, the application of both Mulliken and NPA approaches is essential for revealing the connection between electronic features of a molecule and its reactivity. Moreover, such an integrated approach helps understand better the biological properties, interactions with ligands, and practical uses of molecules in pharmaceuticals. Therefore, in theoretical studies in chemistry, Mulliken and especially NPA methods cannot be overlooked.

Table 2. Mulliken and natural population analysis.

Atom	Mulliken	Natural	Atom	Mulliken	Natural
O1	-0.310269	-0.58519	**C12**	-0.268188	-0.55112
O2	-0.348206	-0.52004	**C13**	-0.134011	-0.15464
O3	-0.350544	-0.64609	**H3**	0.101277	0.17966
O4	-0.357136	-0.52020	**H5**	0.099339	0.18365

O5	-0.400936	-0.76482	**H7**	0.119799	0.20227
C1	0.438478	0.76708	**H10A**	0.131991	0.20482
C2	-0.340055	-0.08678	**H10B**	0.112976	0.18842
C3	0.100755	-0.12004	**H11**	0.123205	0.15041
C4	-0.124093	-0.08610	**H12A**	0.118106	0.19249
C5	-0.100075	-0.28584	**H12B**	0.106322	0.18569
C6	0.175644	0.35948	**H12C**	0.104987	0.18387
C7	-0.075886	-0.25978	**H13A**	0.112842	0.15178
C8	0.180363	0.32484	**H13B**	0.112861	0.15254
C9	0.159711	0.25479	**H13C**	0.134572	0.17204
C10	-0.136653	-0.40562	**H3O**	0.263388	0.46334
C11	0.015767	0.21492	**H5O**	0.233669	0.45417

HS Analysis and Intermolecular Contacts

HS analysis is considered an efficient method for measuring the interactions that exist between molecules of molecular crystals. HSs along with fingerprint plots depicted in this study were obtained through Crystal Explorer 17.5 (Turner *et al*., 2017). The d_{norm} refers to the normalized contact distance and its value can be determined using the following formula:

$$d_{norm} = \frac{d_i - r_i^{vdw}}{r_i^{vdw}} + \frac{d_e - r_e^{vdw}}{r_e^{vdw}}$$

where d_e is the distance between a point in the surface and the closest nucleus that is located outside of the HS, while d_i is the distance between a point in the surface and the closest nucleus located inside the HS; r_i^{vdw} represents the van der Waals radius of the atom that is inside the HS, whereas r_e^{vdw} is the van der Waals radius of the atom that is outside the HS (Kanmazalp *et al*., 2019; Kansız & Dege, 2018).

An analysis of the intermolecular forces in the structure of the molecule was performed utilizing the three-dimensional HS (see Figure 5), plotted according to the d_{norm} parameter. This type

of surface is created through normalization of intermolecular contacts based on van der Waals radii, making it possible to differentiate short- from long-range contacts.

Figure 5. The view of the three-dimensional HS plotted over d_{norm}. Symmetry codes: (i) x-1/2, -y+3/2, -z+1; (ii) x+1,y, z.

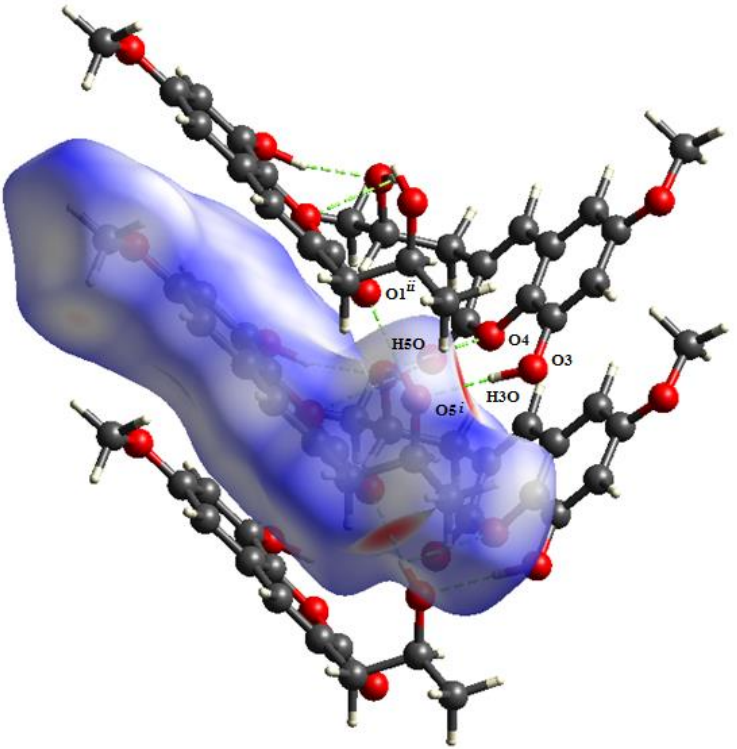

It should be mentioned that the red regions seen on the HS displayed in Figure 5 correspond to intermolecular contacts that can be characterized by the negative value of the d_{norm} parameter, which means that they are shorter than the van der Waals contact distance. It is important to highlight that the presence of such red regions between hydrogen and oxygen atoms demonstrates that the O···H interactions are common in the structure considered. They can be defined as hydrogen bonds and form one of the main

stabilizing forces that have great importance for crystal packing (Spackman *et al*., 2021; Turner *et al*., 2017). As for the white and blue regions identified on the HS, the former correspond to interatomic contacts approaching the van der Waals radii, whereas the latter denote weak interatomic contacts. It can be seen from this color chart that strong (short range) and weak (long range) intermolecular interactions exist in this crystal structure, and that these interactions are responsible for stabilizing the crystal structure through a three-dimensional network (McKinnon *et al*., 2004). HS analysis with respect to d_{norm} has been able to shed light on the type of intermolecular interactions and more importantly on the fact that short range interactions between hydrogen and oxygen atoms are crucial in stabilizing the crystal structure. In this context, the findings provide significant insights into the solid-state properties of the compound (Spackman & Jayatilaka, 2009).

To offer a more comprehensive understanding of the molecular properties related to the compound's intermolecular interactions, different parametric plots of the HS have been assessed simultaneously (Figure 6). With regard to the nature of intermolecular interactions in the crystal structure, d_norm, inner contact distance (d_i), outer contact distance (d_e), shape index, curvedness, and fragment patch analysis surfaces have been considered. Amongst these, although the shape index surface offers important information regarding π-π stacking interactions, the curvedness plot has been used to effectively understand the flatness of the surface and contact zones. On the other hand, fragment patches offer useful information in distinguishing between individual fragment contributions (Turner *et al*., 2017; Spackman *et al*., 2021).

Figure 6. HS analysis of the compound with d_{norm}, d_i, d_e, shape index, curvedness, and fragment patch.

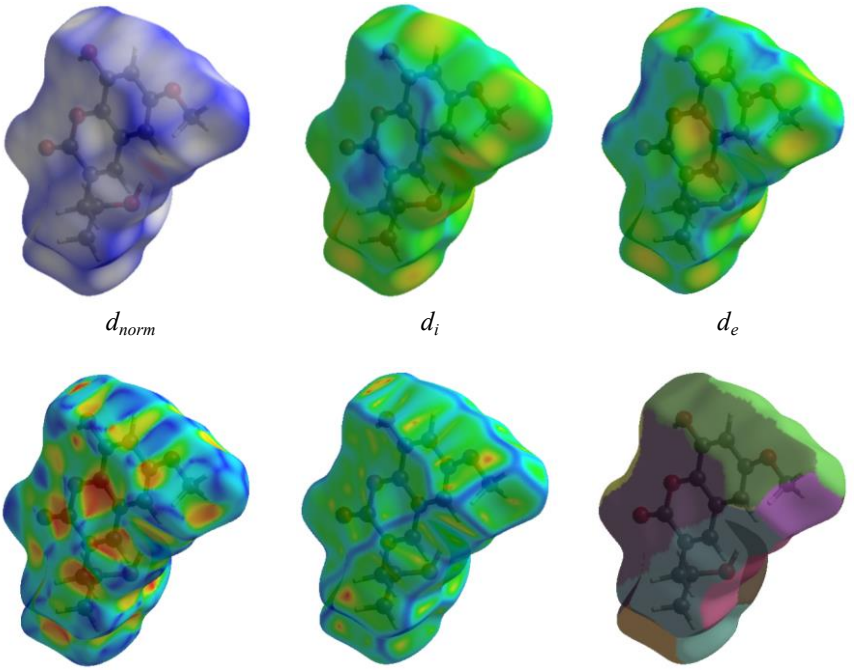

d_{norm} surface constitutes an important factor when assessing the strength and closeness of intermolecular interactions in a given molecule. It was noted in the experiment that the values of d_{norm} surface ranged between -0.6462 and 1.2340. In the event that the value of d_{norm} is negative, then it implies a situation where there is a strong interaction at a contact distance smaller than the van der Walls' contact distance. On the other hand, the situation when the d_{norm} value is positive implies a weak interaction at larger contact distance. This means that the reddish regions in Figure 6 depict strong interactions, white and blue depict moderate and weak interactions respectively. Visualizing the above surfaces is important since they depict the presence and intensity of intermolecular interactions (McKinnon *et al*., 2004; Spackman *et al*., 2021). The d_i and d_e surfaces, representing the inner and outer

contact distances, respectively, play a significant role in understanding the direction and reciprocal nature of interactions. In this case, it is found that d_i values vary from 0.7099 to 2.4256 Å, whereas d_e varies from 0.7097 to 2.3226 Å. These variations mean that there exist strong short range and weaker long range intermolecular interactions between the molecule and its surrounding. Notably, those areas where both low d_i and d_e values coexist have been identified as areas where strong intermolecular interaction takes place (Turner *et al*., 2021). The shape index surface whose value lies within −1.0000 to 1.0000 provides the possibility of identifying concave and convex areas on the molecular surface, allowing analysis of intermolecular geometry complementarity. The characteristic alternating distribution of colors on the surface makes it easy to understand complementary surface geometry, especially where there is π-stacking interaction. The Curvedness surface value falls between −4.0000 and 0.4000. Curvedness is defined as low for wide and flat surface geometries and as high for smaller and sharper geometries. These studies show how surface geometry has a direct correlation with the kind of interactions (Spackman & Jayatilaka, 2009). The fragment patch study (between 0.0000–13.0000) shows that there are intermolecular contacts in certain regions of the surface and that these regions act as interaction centres. This means that there are certain specific regions on the surface where interactions are not randomly distributed. These specific regional concentrations have an important role in influencing crystal packing (Spackman *et al*., 2021). From the above discussion, it can be seen that various types of HS analyses provided in Figure 6 confirm how interactions in the molecule can be studied quantitatively with respect to distance and surface geometry. This is made possible by analyzing the d_{norm}, d_i and d_e parameters along with shape index and curvedness analysis. Thus, there is no doubt that these analyses make considerable contributions to crystal packing and molecular studies.

Detailed investigations of the relative distribution of intermolecular interactions in the crystal structure of the compound were conducted using two-dimensional (2D) fingerprint plots (Figure 7). The fingerprint plots provide information on the ratios of contributions of various contacts towards the total area of the HS as well as their typical distribution pattern, thus making it possible to identify the main mechanisms of interactions in the crystal lattice (Turner *et al*., 2017; McKinnon *et al*., 2004).

Figure 7. The 2D- Fingerprint plots showing the overall contribution to the total HS area and the individual percentages of the diverse intermolecular contacts of the molecule.

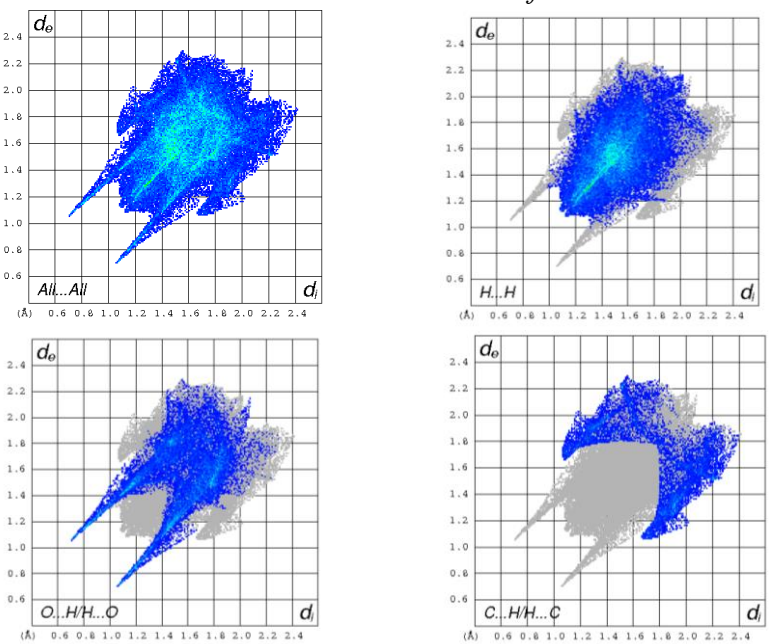

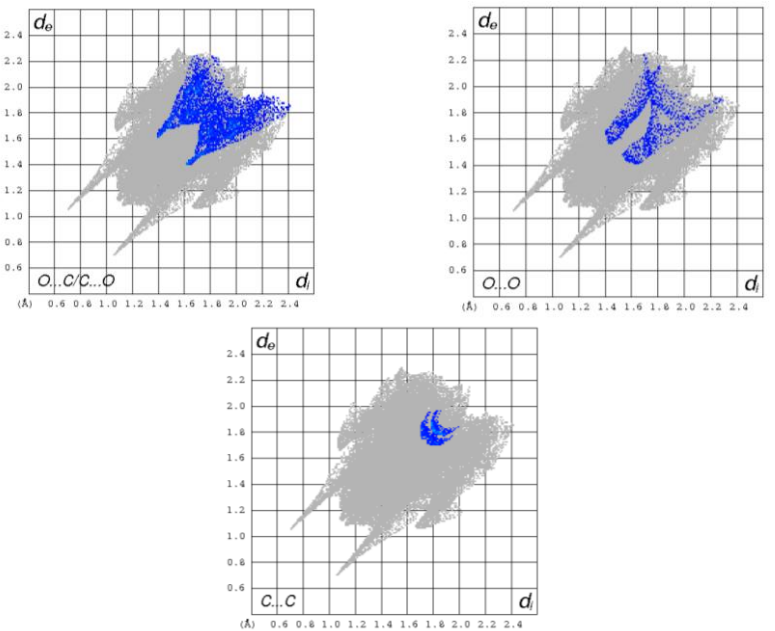

The 2D fingerprint plots provided in Figure 7 demonstrate the quantitative pattern of intermolecular interactions in the crystal structure of the compound. From the results of the analysis, it is evident that H···H bonds are the most dominant interaction type, representing 46.4% of the interactions. The large contribution is attributed to the abundance of hydrogen atoms on the molecular surface, suggesting that van der Waals interactions dominate in the crystal packing. While H···H contacts belong to the category of weak interactions, it is noteworthy that they have been shown to contribute substantially to the stability of the crystal structure because of their significant percentage contribution (Spackman *et al*., 2021; McKinnon *et al*., 2004). The second most dominant interaction type is O···H/H···O contacts, contributing 27.8%. These are direction-dependent and selective interactions associated with hydrogen bonding, involving oxygen and hydrogen atoms. The significant contribution suggests that hydrogen bonds are critical to the crystal structure and provide guidance for

intermolecular ordering (Spackman & Jayatilaka, 2009). If one considers the contacts with lower contribution values, one can notice that C···H/H···C contacts are characterized by 13.9% of contribution value. They may be classified as weak C–H···π or hydrophobic contacts. They provide additional contributions to the three-dimensional structure organization of the crystal. Moreover, O···C/C···O contact contribution of 8.5% reflects the presence of weak directional interactions between oxygen and carbon atoms (Turner *et al*., 2017). Finally, it was stated that O···O (2.2%) and C···C (1.2%) contacts have contribution rates that are extremely low. It is indicative of the limited scope of π–π stacking interactions. The contribution rates of oxygen-oxygen contacts in crystal structure is rather small as well. Thus, the contribution rate of C···C contact points to the absence of strong surface overlap in the studied aromatic system (McKinnon *et al*., 2004). As a result of 2D fingerprint analyses, it is possible to state that the crystal structure formation in question is mainly governed by two factors: weak van der Waals interactions (H···H) and directed hydrogen bonding (O···H/H···O). These two fundamental interaction types play a complementary role in both ensuring structural stability and determining intermolecular ordering. It is important to realize that there are other weak interactions playing an auxiliary role in the framework of this interaction network. Therefore, the percentage contributions gained using 2D fingerprints become indicative of the significance of the intermolecular interactions and contribute substantially to the evaluation of the compound from the viewpoint of crystal engineering. In particular, the method appears superior in terms of identification of interactions, both in their type and relative strength (Turner *et al*., 2017; Spackman *et al*., 2021).

Conclusions

The current research work explores the structural, electronic, and crystal packing features of (*S*)-8-hydroxy-3-(2-hydroxypropyl)-6-methoxy-2*H*-chromen-2-one (Berkecoumarin) compound using a combination of experimental analysis and DFT methods. The findings of the current work are indicative of the validity of the adopted approach and highlight the key aspects related to the behavior of the molecule from the chemical standpoint. Comparisons of the geometrical parameters have shown that computations carried out at B3LYP/6-311(d,p) level demonstrate a high degree of agreement with experimental data obtained via X-ray diffraction method. In other words, the adopted computational method can effectively model the structural behavior of conjugated coumarin molecules. Planarity and extended π-conjugation system are regarded as valuable characteristics of Berkecoumarin in terms of electronic properties and its interaction with biological environment. Analysis of the frontier orbitals of the molecule suggests that the HOMO is distributed over electron-rich zones (mainly near oxygen atoms) and LUMO demonstrates delocalization across the π-system. The large energy gap between HOMO-LUMO orbitals calculated for the compound suggests the high electronic stability and low reactivity of the molecule. This idea is further reinforced by global reactivity parameters which clearly indicate the balanced electronegativity, high chemical rigidity, and poor molecular flexibility of the compound. It follows from the above analysis that Berkecoumarin is indeed a stable molecule with controlled reactivity. As per MEP analysis of the molecule, there is an electrostatic charge distribution observed in the molecule where oxygen atoms are the negative potential regions being prone to electrophilic attack. Hydroxyl hydrogen atoms on the other hand form the positive potential region with hydrogen bond donating property. Results obtained from Mulliken

and NPA analysis also reinforce the above findings with oxygen atoms behaving as strong nucleophilic centers and charge distribution being non-uniform in nature. Since NPA charge distribution values prove to be more accurate, NPA technique is thus a better choice for studying reactivity parameters. The HS analysis and 2D fingerprint plots have quantitatively and graphically demonstrated the nature of intermolecular interactions within the crystal structure. From the results of this analysis, it can be observed that the crystal packing depends on H···H van der Waals interactions (46.4%) and O···H/H···O hydrogen bonds (27.8%). The above interactions complement each other to stabilize the crystal lattice. Other lower-frequency C···H, O···C, and other intermolecular interactions act as auxiliary contacts to these interactions. Additionally, shape index and curvedness analyses have detailed the intermolecular geometric fit and surface character.

References

Aswathy, U., Pandey, A. K., Sharma, P., Sreekumar, N., & Kumar, S. (2021). Emerging industrial applications of microalgae: Challenges and future perspectives. *Systems Microbiology and Biomanufacturing*, *1*(4), 411-431. https://doi.org/10.1007/s43393-021-00038-8

Becke, A. D. (1993). Density-functional thermochemistry. III. The role of exact exchange. *The Journal of Chemical Physics*, *98*(7), 5648-5652. https://doi.org/10.1063/1.464913

Chakraborty, D., & Chattaraj, P. K. (2021). Conceptual density functional theory based electronic structure principles. *Chemical Science*, *12*, 6264 - 6279. https://doi.org/10.1039/D0SC07017C

Çelik, K., & Ongun, T. (2007). The influence of certain physical and chemical variables on the seasonal dynamics of phytoplankton assemblages of a source inlet and the outlet of the shallow hypertrophic Lake Manyas, Turkey. *Turkish Journal of Botany*, *31*(6), 485-493.

Decato, D., Palatinus, L., Stierle, A., & Stierle, D. (2024). Absolute structure determination of Berkecoumarin by X-ray and electron diffraction. *Acta crystallographica. Section C*, *Structural chemistry*, *80*(5), 143-147. https://doi.org/10.1107/S2053229624003061

Deniz, F., & Tezel Ersanlı, E. (2016a). Simultaneous bioremoval of two unsafe dyes from aqueous solution using a novel green composite biosorbent. *Microchemical Journal*, *128*, 312-319. https://doi:10.1016/j.microc.2016.05.012

Deniz, F., & Tezel Ersanlı, E. (2016b). Removal of colorant from simulated wastewater by phyco-composite material: Equilibrium, kinetic and mechanism studies in a lab-scale application. *Journal of Molecular Liquids*, *220*, 120-128. https://doi.org/10.1016/j.molliq.2016.04.081

Deniz, F., & Tezel Ersanlı, E. (2018a). An ecofriendly approach for bioremediation of contaminated water environment: Potential contribution of a coastal seaweed community to environmental improvement. *International Journal of Phytoremediation*, *20*(3), 256-263. https://doi.org/10.1080/15226514.2017.1374335

Deniz, F., & Tezel Ersanlı, E. (2018b). A natural macroalgae consortium for biosorption of copper from aqueous solution: Optimization, modeling and design studies. *International Journal of Phytoremediation*, *20*(4), 362-368. https://doi.org/10.1080/15226514.2017.1393387

Deniz, F., & Tezel Ersanlı, E. (2020a). An effectual biosorbent substance for removal of manganese ions from aquatic environment: A promising environmental remediation study with activated coastal waste of *Zostera marina* plant. *BioMed Research International*, *2020*(1), 7806154, 1-8. https://doi.org/10.1155/2020/7806154

Deniz, F., & Tezel Ersanlı, E. (2020b). A low-cost and eco-friendly biosorbent material for effective synthetic dye removal from aquatic environment: Characterization, optimization, kinetic, isotherm and thermodynamic studies. *International Journal of Phytoremediation*, *22*(4), 353-362. https://doi.org/10.1080/15226514.2019.1663485

Deniz, F., & Tezel Ersanli, E. (2021a). A renewable biosorbent material for green decontamination of heavy metal pollution from aquatic medium: A case study on manganese removal. *International Journal of Phytoremediation*, *23*(3), 231-237. https://doi.org/10.1080/15226514.2020.1807905

Deniz, F., & Tezel Ersanli, E. (2021b). Purification of malachite green as a model biocidal agent from aqueous system by using a natural widespread coastal biowaste (*Zostera marina*). *International Journal of Phytoremediation*, *23*(7), 772-779. https://doi.org/10.1080/15226514.2020.1857684

Deniz, F., & Tezel Ersanlı, E. (2022). A novel biowaste-based biosorbent material for effective purification of methylene blue from water environment. *International Journal of Phytoremediation*, *24*(12), 1243-1250. https://doi.org/10.1080/15226514.2021.2025039

Dennington, R., Keith, T., & Millam, J. (2007). *GaussView* (Version 4.1.2). Semichem Inc.

Domingo, L. R., Ríos-Gutiérrez, M., & Pérez, P. (2016). Applications of the conceptual density functional theory indices to organic chemistry reactivity. *Molecules*, *21*(6), 748. https://doi.org/10.3390/molecules21060748

Frisch, M. J., Trucks, G. W., Schlegel, H. B., Scuseria, G. E., Robb, M. A., Cheeseman, J. R., Montgomery, J. A., Jr., Vreven, T., Kudin, K. N., Burant, J. C., Millam, J. M., Iyengar, S. S., Tomasi, J., Barone, V., Mennucci, B., Cossi, M., Scalmani, G., Rega, N., Petersson, G. A., Nakatsuji, H., Hada, M., Ehara, M., Toyota, K., Fukuda, R., Hasegawa, J., Ishida, M., Nakajima, T., Honda, Y., Kitao, O., Nakai, H., Klene, M., Li, X., Knox, J. E., Hratchian, H. P., Cross, J. B., Bakken, V., Adamo, C., Jaramillo, J., Gomperts, R., Stratmann, R. E., Yazyev, O., Austin, A. J., Cammi, R., Pomelli, C., Ochterski, J. W., Ayala, P. Y., Morokuma, K., Voth, G. A., Salvador, P., Dannenberg, J. J., Zakrzewski, V. G., Dapprich, S., Daniels, A. D., Strain, M. C., Farkas, O., Malick, D. K., Rabuck, A. D., Raghavachari, K., Foresman, J. B., Ortiz, J. V., Cui, Q., Baboul, A. G., Clifford, S., Cioslowski, J., Stefanov, B. B., Liu, G., Liashenko, A., Piskorz, P., Komaromi, I., Martin, R. L., Fox, D. J., Keith, T., Al-Laham, M. A., Peng, C. Y., Nanayakkara, A., Challacombe, M., Gill, P. M. W., Johnson, B., Chen, W., Wong, M. W., Gonzalez, C., & Pople, J. A. (2004). *Gaussian 03*, Revision C.02. Gaussian, Inc.

Frisvad, J. C., & Samson, R. A. (2004). Polyphasic taxonomy of *Penicillium* subgenus *Penicillium* - A guide to identification of food and air-borne terverticillate penicillia and their mycotoxins. *Studies in Mycology*, *49*, 1-52.

Geerlings, P., De Proft, F., & Langenaeker, W. (2003). Conceptual density functional theory, *Chemical Reviews*, *103*, 1793-1873. https://doi.org/10.1021/cr990029p

Hasırcı Mustak, S., & Tezel Ersanlı, E. (2015). Spatial and temporal characterization of the physicochemical parameters and phytoplankton assemblages in Dodurga Reservoir (Sinop, Turkey). *Turkish Journal of Botany*, *39*(3), 547-554. https://doi.org/10.3906/bot-1407-32

Kanmazalp, S. D., Macit, M., & Dege, N. (2019). Hirshfeld surface, crystal structure and spectroscopic characterization of (*E*)-4-(diethylamino)-2-((4-phenoxyphenylimino) methyl) phenol with DFT studies. *Journal of Molecular Structure*, *1179*, 181-91. https://doi.org/10.1016/j.molstruc.2018.11.001

Kansız, S., & Dege, N. (2018). Synthesis, crystallographic structure, DFT calculations and Hirshfeld surface analysis of a fumarate bridged Co(II) coordination polymer. *Journal of Molecular Structure*, 2018, *1173*, 42-51. https://doi.org/10.1016/j.molstruc.2018.06.071

Kumar, A., Baccoli, R., Fais, A., Cincotti, A., Pilia, L., & Gatto, G. (2020). Substitution effects on the optoelectronic properties of coumarin derivatives. *Applied Sciences*, *10*(1), 144. https://doi.org/10.3390/app10010144

Lee, C. T., Yang, W. T., & Parr, R. G. (1988). Development of the Colle-Salvetti correlation-energy formula into a functional of the electron density. *Physical Review B*, *37*, 785-789. https://doi.org/10.1103/PhysRevB.37.785

Lu, T., & Chen, F. (2012). Multiwfn: A multifunctional wavefunction analyzer. *Journal of Computational Chemistry*, *33*(5), 580–592. https://doi.org/10.1002/jcc.22885

McKinnon, J. J., Spackman, M. A., & Mitchell, A. S. (2004). Novel tools for visualizing and exploring intermolecular interactions in molecular crystals. *Acta Crystallographica Section*

B, *Structural Science*, *60*(6), 627-668. https://doi.org/10.1107/S0108768104020300

Murray, J. S., & Politzer, P. (2017). Molecular electrostatic potentials and noncovalent interactions. *WIREs Computational Molecular Science*, *7*, e1326. https://doi.org/10.1002/wcms.1326

Parr, R.G., & Yang, W. (1989). *Density Functional Theory of Atoms and Molecules*. Oxford University Press, New York.

Pitt, J. I., Samson, R. A., & Frisvad, J. C. (2000). *List of accepted species and their synonyms in the Family Trichocomaceae*. In: Samson, R. A. & Pitt, J. I., Eds., Integration of Modern Taxonomic Methods for *Penicillium* and *Aspergillus* Plenum Press, New York, 9-49.

Politzer, P., Murray, J. S., & Clark, T. (2013). Halogen bonding and other σ-hole interactions: A perspective. *Physical Chemistry Chemical Physics*, *15*, 11178-11189. https://doi.org/10.1039/c3cp00054k

Raja, H. A., Miller, A. N., Pearce, C. J., & Oberlies, N. H. (2017). Fungal identification using molecular tools: A Primer for the natural products research community. *Journal of Natural Products*, *80*, 756-770. https://doi.org/10.1021/acs.jnatprod.6b01085

Roy, K., Kar, S., & Das, R. N. (2015). *Understanding the Basics of QSAR for Application in Pharmaceutical Science and Risk Assessment*. Volume 6, Academic Press, London, 191-228.

Sarı, A., & Tüzen, M. (2008). Biosorption of Pb(II) and Cd(II) from aqueous solution using green alga (*Ulva lactuca*) biomass. *Journal of Hazardous Materials*, *152*(1), 302-308. https://doi.org/10.1016/j.jhazmat.2007.06.097

Serrano, A., Palacios, C., Roy, G., Cespón, C., Villar, M. L., Nocito, M., & González-Porqué, P. (1998). Derivatives of gallic acid induce apoptosis in tumoral cell lines and inhibit lymphocyte proliferation. *Archives of Biochemistry and Biophysics*, *350*(1), 49-54. https://doi.org/10.1006/abbi.1997.0474

Solak, C. N., Peszek, Ł., Yilmaz, E., Ergül, H. A., Kayal, M., Ekmekçi, F., Várbíró, G., Yüce, A. M., Canli, O., Binici, M. S., & Ács, É. (2020). Use of diatoms in monitoring the Sakarya River Basin, Turkey. *Water*, *12*(3), 703. https://doi.org/10.3390/w12030703

Spackman, M. A., & Jayatilaka, D. (2009). Hirshfeld Surface Analysis. *CrystEngComm*, *11*, 19-32. http://dx.doi.org/10.1039/B818330A

Spackman, P. R., Turner, M. J., McKinnon, J. J., Wolff, S. K., Grimwood, D. J., Jayatilaka, D., & Spackman, M. A. (2021). CrystalExplorer: A program for Hirshfeld surface analysis, visualization and quantitative analysis of molecular crystals. *Journal of Applied Crystallography*, *54*(3), 1006-1011. https://doi.org/10.1107/S1600576721002910

Tezel Ersanlı, E., & Gönülol, A. (2014). Phytoplankton dynamics and some physicochemical variables in Cakmak Reservoir, Samsun, Turkey. *MANAS Journal of Agriculture and Life Sciences*, *4*(1), 17-25.

Tezel Ersanlı, E., & Hasırcı, S. (2013). The relationship between environmental variables and the vertical and horizontal assemblages of phytoplankton in Erfelek Reservoir in Sinop, Turkey. *Turkish Journal of Botany*, *37*(4), 715-726. https://doi.org/10.3906/bot-1207-21

Tezel Ersanlı, E., & Hasırcı Mustak, S. (2017). Distribution dynamics of vegetative cells and cyst of *Ceratium hirundinella* in

two reservoirs, Turkey. Süleyman Demirel University *Journal of Natural and Applied Sciences*, *21*(1), 247-253. https://doi.org/10.19113/sdufbed.99878

Tezel Ersanlı, E., & Öztürk, R. (2017). Ecological and statistical evaluation of algal flora and water quality of Karasu Stream. *KSU Journal of Natural Sciences*, *20*(3), 193-200. https://doi.org/10.18016/ksudobil.264177

Turner, M. J., McKinnon, J. J., Wolff, S. K., Grimwood, D. J., Spackman, P. R., Jayatilaka, D., & Spackman, M. A. (2017). *CrystalExplorer17 (Version 17.5)*. University of Western Australia.

Yılmaz, N., Yardımcı, C. H., Elhag, M., & Dumitrache, C. A. (2018). Phytoplankton composition and water quality of Kamil Abduş Lagoon (Tuzla Lake), Istanbul-Turkey. *Water*, *10*(5), 603. https://doi.org/10.3390/w10050603


BİDGE